

# 1 Rapid transition in winter aerosol composition in Beijing from 2014 to 2 2017: response to clean air actions

3 Haiyan Li<sup>1,a</sup>, Jing Cheng<sup>2</sup>, Qiang Zhang<sup>2</sup>, Bo Zheng<sup>1</sup>, Yuxuan Zhang<sup>2</sup>, Guangjie Zheng<sup>1</sup>, Kebin He<sup>1,3</sup>

4 <sup>1</sup> State Key Joint Laboratory of Environment Simulation and Pollution Control, School of Environment, Tsinghua University,  
5 Beijing 100084, China

6 <sup>2</sup> Ministry of Education Key Laboratory for Earth System Modeling, Department of Earth System Science, Tsinghua University,  
7 Beijing 100084, China

8 <sup>3</sup> State Environmental Protection Key Laboratory of Sources and Control of Air Pollution Complex, Tsinghua University, Beijing  
9 100084, China

10 <sup>a</sup>present address: Institute for Atmospheric and Earth System Research/Physics, Faculty of Science, University of Helsinki, 00014  
11 Helsinki, Finland

12 *Correspondence:* Qiang Zhang ([qiangzhang@tsinghua.edu.cn](mailto:qiangzhang@tsinghua.edu.cn))

13 **Abstract.** The clean air actions implemented by the Chinese government in 2013 have led to significantly improved air quality in  
14 Beijing. In this work, we combined the in-situ measurements of the chemical components of submicron particles (PM<sub>1</sub>) in Beijing  
15 during the winters of 2014 and 2017 and a regional chemical transport model to investigate the impact of clean air actions on  
16 aerosol chemistry and quantify the relative contributions of anthropogenic emissions, meteorological conditions, and regional  
17 transport to the changes in aerosol chemical composition from 2014 to 2017. We found that the average PM<sub>1</sub> concentration in  
18 winter in Beijing decreased by 49.5% from 2014 to 2017 (from 66.2  $\mu\text{g m}^{-3}$  to 33.4  $\mu\text{g m}^{-3}$ ). Sulfate exhibited a much larger decline  
19 than nitrate and ammonium, which led to a rapid transition from sulfate-driven to nitrate-driven aerosol pollution during the  
20 wintertime. Organic aerosol (OA), especially coal combustion OA, and black carbon also showed large decreasing rates, indicating  
21 the effective emission control of coal combustion and biomass burning. The decreased sulfate contribution and increased nitrate  
22 fraction were highly consistent with the much faster emission reductions in sulfur dioxide (SO<sub>2</sub>) due to phasing out coal in Beijing  
23 compared to reduction in nitrogen oxides emissions estimated by bottom-up inventory. The chemical transport model simulations  
24 with these emission estimates reproduced the relative changes in aerosol composition and suggested that the reduced emissions in  
25 Beijing and its surrounding regions played a dominant role. The variations in meteorological conditions and regional transport  
26 contributed much less to the changes in aerosol concentration and its chemical composition during 2014-2017 compared to the  
27 decreasing emissions. Finally, we speculated that changes in precursor emissions possibly altered the aerosol formation  
28 mechanisms based on ambient observations. The observed explosive growth of sulfate at a relative humidity (RH) greater than 50%  
29 in 2014 was delayed to a higher RH of 70% in 2017, which was likely caused by the suppressed sulfate formation through  
30 heterogeneous reactions due to the decrease of SO<sub>2</sub> emissions. Thermodynamic simulations showed that the decreased sulfate and  
31 nitrate concentrations have lowered the aerosol water content, particle acidity, and ammonium particle fraction. The results in this  
32 study demonstrated the response of aerosol chemistry to the stringent clean air actions and identified that the anthropogenic  
33 emission reductions are a major driver, which could help to further guide air pollution control strategies in China.

## 34 1 Introduction

35 Beijing, the capital of China, is one of the most heavily polluted cities in the world (Lelieveld et al., 2015), and it frequently  
36 experiences severe and persistent haze pollution episodes in winter (Guo et al., 2014). For example, in January 2013, the daily  
37 concentration of ambient particles with an aerodynamic diameter less than 2.5  $\mu\text{m}$  (PM<sub>2.5</sub>) reached a record high of 569  $\mu\text{g m}^{-3}$  in  
38 Beijing (Ferreri et al., 2018), which was over 20 times higher than the World Health Organization standard (25  $\mu\text{g m}^{-3}$  for daily

average  $\text{PM}_{2.5}$ ). As a complex mixture of many different components, ambient aerosols have a range of chemical compositions and originate from various emission sources and formation processes in the atmosphere (Seinfeld and Pandis, 2012). The adverse effects of aerosols on visibility (Pui et al., 2014), climate (IPCC, 2013), and human health (Pope et al., 2009) are intrinsically related to the chemical composition of particles.

To tackle severe aerosol pollution, the Chinese State Council implemented the Air Pollution Prevention and Control Action Plan (denoted as clean air actions) in September 2013, which is the most stringent pollution mitigation policy ever in China. As a consequence, China's anthropogenic emissions have declined by 59% for  $\text{SO}_2$ , 21% for  $\text{NO}_x$ , 32% for organic carbon (OC), and 28% for black carbon (BC) during 2013-2017 (Zheng et al., 2018). The annual average  $\text{PM}_{2.5}$  concentration in Beijing decreased by 35.6% from 2013 to 2017, reaching  $58 \mu\text{g m}^{-3}$  in 2017. Combining the bottom-up emission inventory and chemical transport model simulations, our recent study (Cheng et al., 2019) quantified the relative contributions of meteorological conditions, emission reductions from surrounding regions, and emission reductions from local sources to the decrease in  $\text{PM}_{2.5}$  concentration in Beijing during 2013-2017. While changes in meteorological conditions partially explained air quality improvement in Beijing in 2017, local and regional emission controls played major roles. In addition, the aerosol chemical composition is expected to change correspondingly due to the rapid reductions in precursor emissions, which is not well understood yet because the chemical components of  $\text{PM}_{2.5}$  are not measured by China's monitoring network. A few studies have examined the change in aerosol composition in Beijing after 2013, including a semicontinuous measurement of carbonaceous aerosols during 2013-2018 (Ji et al., 2019) and an aerosol mass spectrometry study comparing aerosol composition and size distribution between 2014 and 2016 (Xu et al., 2019). However, neither performed a comprehensive assessment of all the main factors affecting aerosol concentration and its composition. A deep understanding of how the aerosol composition has changed since the clean air actions were activated and the possible linkage between them is urgently needed.

The chemical composition of  $\text{PM}_{2.5}$  is mainly affected by the following factors: precursor emissions, meteorological conditions, atmospheric chemical reactions, and regional transport and deposition. Emissions are typically the main driver of aerosol composition changes. During 2005-2012, the sulfate concentration in China decreased, while the nitrate concentration increased, which was caused by the considerable reduction in  $\text{SO}_2$  emissions but limited control of  $\text{NO}_x$  (Geng et al., 2017). Based on the measurements of organic aerosol (OA) composition in Beijing, a larger decrease in secondary OA than primary OA was found during the 2014 Asia-Pacific Economic Cooperation summit due to the strict emission controls (Sun et al., 2016). Meteorological conditions affect aerosol composition by changing emissions, chemical reactions, and transport and deposition processes (Mu and Liao, 2014). For example, increases in relative humidity (RH) enhance the secondary formation of sulfate through heterogeneous reactions (Zheng et al., 2015; Cheng et al., 2016), and decreases in temperature favor particulate nitrate formation by facilitating gas-to-particle partitioning (Pye et al., 2009; Li et al., 2018). With chemical transport model simulations in China for the years 2004-2012, Mu and Liao (2014) demonstrated that due to the large variations in meteorological parameters in North China, all aerosol species showed large corresponding interannual variations. Furthermore, aerosol characteristics in Beijing are influenced by regional transport from adjacent polluted regions. Polluted air masses from the southern regions contributed more secondary inorganic aerosols (SIAs) than primary aerosols in Beijing (Zhang et al., 2014; Du et al., 2018).

Following our previous work (Cheng et al., 2019), the main objective of this study is to investigate the impact of clean air actions on changes in aerosol chemical composition from 2014 to 2017. With both the in-situ observations of aerosol species in Beijing during the winters of 2014 and 2017 and model simulations for the corresponding periods, this work provides the opportunity for a detailed evaluation of the underlying drivers. First, changes in aerosol characteristics are illustrated for inorganics and organics by comparing aerosol measurements in 2014 and 2017. Then, the relative importance of different factors in varying aerosol composition is assessed by combining direct observations and model simulations, including synoptic conditions, emission changes,

79 regional transport and formation mechanisms. Last, we show that the transition in aerosol characteristics influenced particle  
80 properties, such as aerosol water content (AWC) and particle acidity, which in turn affects secondary aerosol formation.

## 81 **2 Experimental methods**

### 82 **2.1 Ambient sampling and instrumentation**

83 Online aerosol measurements were performed in urban Beijing during the winters of 2014 (from 6 December 2014 to 27 February  
84 2015) and 2017 (from 11 December 2017 to 2 February 2018). The sampling site is located on the roof of a three-story building  
85 on the campus of Tsinghua University (40.0° N, 116.3° E), which is surrounded by school and residential areas. No major industrial  
86 sources are situated nearby. An Aerodyne Aerosol Chemical Speciation Monitor (ACSM) was deployed for the real-time chemical  
87 observations of nonrefractory PM<sub>1</sub> (NR-PM<sub>1</sub>), including organics, sulfate, nitrate, ammonium, and chloride. A detailed description  
88 of the instrument can be found in Ng et al. (2011a). The mass concentration of BC in PM<sub>1</sub> was measured using a multiangle  
89 absorption photometer (MAAP, model 5012; Petzold and Schönlinner, 2004). In addition, the total PM<sub>2.5</sub> mass was simultaneously  
90 recorded with a PM-712 monitor based on the  $\beta$ -ray absorption method (Kimoto Electric Co., Ltd., Japan). For gaseous species,  
91 the mixing ratios of SO<sub>2</sub>, NO<sub>x</sub>, CO, and O<sub>3</sub> were monitored by a suite of commercial gas analyzers (Thermo Scientific). The  
92 meteorological parameters, including temperature, RH, wind speed (WS), and wind direction (WD), were obtained from an  
93 automatic meteorological observation instrument (MILOS520, VAISALA Inc., Finland).

### 94 **2.2 ACSM data analysis**

95 The ACSM data were analyzed using the standard analysis software within Igor Pro (WaveMetrics, Inc., Oregon USA). Default  
96 relative ionization efficiencies (RIEs) were applied to organics (1.4), nitrate (1.1), and chloride (1.3), while the RIEs of ammonium  
97 and sulfate were experimentally determined through calibrations with pure ammonium nitrate and ammonium sulfate, respectively.  
98 A composition-dependent collection efficiency (CE) algorithm was used to account for the incomplete detection of aerosol particles  
99 (Middlebrook et al., 2012). As shown in Fig. S1, the total measured PM<sub>1</sub> mass (NR-PM<sub>1</sub> plus BC) correlated well with the PM<sub>2.5</sub>  
100 obtained from PM-712 ( $r^2 = 0.80$  and  $0.87$  for 2014 and 2017, respectively). On average, PM<sub>1</sub> accounted for 68% and 80% of the  
101 total PM<sub>2.5</sub> in Beijing during the winters of 2014 and 2017.

102 The ACSM provides unit-mass-resolution mass spectra of submicron particles, facilitating source apportionment via factor analysis.  
103 In this study, positive matrix factorization (PMF) was implemented to resolve OA into various sources using a multilinear engine  
104 (ME-2; Paatero, 1999) via the SoFi toolkit (Source Finder; Canonaco et al., 2013). The so-called  $a$  value approach allows for the  
105 introduction of a priori factor profile or time series to reduce the rotational ambiguity and obtain a unique solution. The spectra  
106 and error matrices of organics were pretreated based on the procedures given by Ulbrich et al. (2009) and Zhang et al. (2011). Ions  
107 larger than  $m/z$  120 were not considered in this study given the interferences of the internal standard of naphthalene at  $m/z$  127-  
108 129, the low signal-to-noise ratio of larger ions, and their low contributions to OA loading. For the winter of 2014, a reference  
109 hydrocarbon-like OA (HOA) profile from Ng et al. (2011b) was introduced into the ME-2 analysis to constrain the model  
110 performance, varying  $a$  values from 0 to 1. Following the guidelines by Canonaco et al. (2013) and Crippa et al. (2014), an optimal  
111 solution with four factors was finally accepted, with an  $a$  value of 0. Detailed evaluation of the factor time series, mass spectra,  
112 and diurnal patterns with different  $a$  values can be found in the Supplement (Figs. S2-10). Figure S11 shows the source  
113 apportionment results with three primary factors, i.e., HOA, coal combustion OA (CCOA), and biomass burning OA (BBOA), and  
114 one secondary factor, oxygenated OA (OOA). For the 2017 dataset, the mass spectral profiles of HOA, CCOA, and BBOA from  
115 the ME-2 analysis of 2014 were adopted to constrain the model performance. Similarly, a four-factor solution with HOA, BBOA,

116 CCOA, and OOA was selected for the winter of 2017, which allowed a better comparison of the OA sources between 2014 and  
117 2017.

### 118 2.3 WRF-CMAQ model

119 The Weather Research and Forecasting (WRF) model, version 3.8, and the Community Multiscale Air Quality (CMAQ) model,  
120 version 5.1, were applied to evaluate the impact of meteorological changes, regional transport and emission variations on the PM<sub>2.5</sub>  
121 concentration in Beijing in winter. The simulated area was designed as three nested domains, and the innermost area covered  
122 Beijing and its surrounding regions (including Tianjin, Hebei, Shanxi, Henan, Shandong and Inner Mongolia), with a horizontal  
123 resolution of 4 km × 4 km. The simulated period basically followed the observation time, which covered December 2014 – February  
124 2015 and December 2017 – February 2018. A one-month spin-up was applied in each simulation.

125 The WRF model is driven by the National Centers for Environmental Prediction Final Analysis (NCEP-FNL) reanalysis data,  
126 which then provided the meteorological fields for the CMAQ model. We used CB05 and AERO6 as the gas and particulate matter  
127 chemical mechanisms, respectively. The in-line windblown dust and photolytic rate calculation modules were also adopted to  
128 improve the simulation. The chemical initial and boundary conditions originated from the interpolated outputs of the Goddard  
129 Earth Observing System with chemistry (GEOS-Chem) model (Bay et al., 2001).

130 The anthropogenic emission inventory for Beijing was taken from the Beijing Municipal Environmental Monitoring Center  
131 (BMEMC), which was documented and analyzed in Cheng et al. (2019), while the emission inventory outside Beijing was provided  
132 by the Multi-resolution Emission Inventory for China (MEIC) (<http://www.meicmodel.org>; Zheng et al., 2018) and the MIX  
133 emission inventory for the other Asian countries (M. Li et al., 2017). The biogenic emissions were obtained by the Model of  
134 Emission of Gases and Aerosols from Nature (MEGAN v2.1); however, open biomass burning was not considered in this work.  
135 Detailed model configurations and validations can be found in Cheng et al. (2019), and the simulated results well reproduced the  
136 temporal and spatial distributions and variations in PM<sub>2.5</sub> in Beijing and its surrounding areas. In this study, we evaluated the model  
137 performance by comparing the simulated PM<sub>2.5</sub> concentrations and compositions in Beijing with observation data. The hourly  
138 observed PM<sub>2.5</sub> concentrations were collected from the Beijing Municipal Environmental Protection Bureau; and the observed  
139 PM<sub>2.5</sub> compositions came from the Surface PARTiculate mAtter Network (SPARTAN, [www.spartan-network.org](http://www.spartan-network.org)). We also  
140 compared the simulated PM<sub>2.5</sub> compositions with the observed PM<sub>1</sub> species from this work. The average simulated PM<sub>2.5</sub> in Beijing  
141 decreased from 91.5 (winter of 2014) to 52.5 (winter of 2017)  $\mu\text{g m}^{-3}$ , with a total decrease of 39  $\mu\text{g m}^{-3}$ , while the observed PM<sub>2.5</sub>  
142 varied from 81.9 to 40.6  $\mu\text{g m}^{-3}$ , decreasing by 41.3  $\mu\text{g m}^{-3}$ . Generally, the simulated and observed PM<sub>2.5</sub> (24-hour averages) in  
143 Beijing agreed well. The time series comparison and detailed monthly descriptive statistic of the observed and CMAQ-simulated  
144 PM<sub>2.5</sub> concentrations can be found in Fig. S12 and Table S1. For PM<sub>2.5</sub> compositions, the Pearson correlation coefficients between  
145 simulated PM<sub>2.5</sub> and observed PM<sub>1</sub> components were all above 0.7 (Table S2a), indicating that the model simulations could well  
146 reproduce the species variations. Detailed comparisons of the simulated and observed PM<sub>2.5</sub> components were listed in Table S2b.  
147 We designed six simulation cases to investigate the impact of meteorological and emission variations. Two base cases were driven  
148 by the actual emission inventory and meteorological conditions in the winter of 2014 (case A) and winter of 2017 (case B). Cases  
149 C and D were designed to quantify the impact of meteorological changes; case C was simulated with the emissions in 2014 and  
150 meteorological conditions of 2017, while case D used the 2017 emissions and 2014 meteorological conditions. Therefore, the  
151 differences between A and C or between B and D show the influence of meteorological conditions, and the differences between A  
152 and D or between B and C correspond to the contributions of emission variations. We used the averaged differences as the final  
153 impacts. Cases E and F were developed to evaluate the effect of regional transport on PM<sub>2.5</sub> variations in Beijing in the winter of  
154 2014 (E) and winter of 2017 (F). In these two cases, the emissions in Beijing were set to zero, while the regional emissions

remained at the actual level. The balances between *A* and *E* or between *B* and *F* represent the contributions of regional transport to the PM<sub>2.5</sub> concentration in Beijing during the corresponding periods.

## 2.4 Clustering analysis of back trajectories

The Hybrid Single Particle Lagrangian Integrated Trajectory (HYSPLIT) model was conducted to calculate the back trajectories of air masses arriving in Beijing during the observation periods in 2014 and 2017. The meteorological input was downloaded from the National Oceanographic and Atmospheric Administration (NOAA) Air Resource Laboratory Archived Global Data Assimilation System (GDAS) (<ftp://arlftp.arlhq.noaa.gov/pub/archives/>). Each trajectory was run for three days, with a time resolution of 1 hour, and the initialized height was 100 m above ground level. In total, 2108 and 1292 trajectories were obtained for the winters of 2014 and 2017, respectively. Based on the built-in clustering calculation, the trajectories were then classified into different groups to represent the main airflows influencing the receptor site. Finally, the optimal 5-cluster and 7-cluster solutions were adopted for the winters of 2014 and 2017, respectively. Details are shown in Fig. S13.

## 2.5 ISORROPIA-II equilibrium calculation

The ISORROPIA-II thermodynamic model was used to investigate the effects of particle chemical composition on aerosol properties, i.e., particle pH, AWC, and the partitioning of semivolatile species (Fountoukis and Nenes, 2007). The model computes the equilibrium state of an NH<sub>4</sub><sup>+</sup>-SO<sub>4</sub><sup>2-</sup>-NO<sub>3</sub><sup>-</sup>-Cl<sup>-</sup>-Na<sup>+</sup>-Ca<sup>2+</sup>-K<sup>+</sup>-Mg<sup>2+</sup>-H<sub>2</sub>O inorganic aerosol system with its corresponding gases (Fountoukis and Nenes, 2007). When running the ISORROPIA-II model, it is assumed that aerosols are internally mixed and composed of a single aqueous phase. The validity of these assumptions has been evaluated by a number of studies in various locations (Guo et al., 2015; Weber et al., 2016; M.X. Liu et al., 2017; Li et al., 2018).

The model was run in the forward mode by assuming that aerosol solutions were metastable. The forward mode calculates the gas-particle equilibrium partitioning with the total concentrations of both gas and particle phase species. Compared to the reverse mode using only aerosol phase compositions, calculations with the forward mode are affected much less by the measurement errors (Hennigan et al., 2015; Guo et al., 2017a; Song et al., 2018). Particle water associated with OA was not considered in this study given its minor effects. M. X. Liu et al. (2017) showed that organic matter (OM)-induced particle water accounted for only 5% of the total AWC in Beijing. Up to now, there are no observational data showing whether aerosols are in a metastable (only liquid) or stable (solid plus liquid) state in Beijing in winter (Song et al., 2018). According to previous studies, at low RH (RH < 20% or 30%), aerosols are less likely to be in a completely liquid state (Fountoukis and Nenes, 2007; Guo et al., 2016, 2017). Therefore, periods with RH < 30% were excluded in this study. The effects of nonvolatile cations (i.e., Na<sup>+</sup>, K<sup>+</sup>, Ca<sup>2+</sup>, Mg<sup>2+</sup>) are not considered in this study because the fraction of nonvolatile cations in PM<sub>1</sub> in Beijing is generally negligible compared to SO<sub>4</sub><sup>2-</sup>, NO<sub>3</sub><sup>-</sup>, and NH<sub>4</sub><sup>+</sup> (Sun et al., 2014). Although nonvolatile nitrate may exist in ambient particles as Ca(NO<sub>3</sub>)<sub>2</sub> and Mg(NO<sub>3</sub>)<sub>2</sub>, Ca<sup>2+</sup> and Mg<sup>2+</sup> are mainly abundant at sizes above 1 μm (Zhao et al., 2017). In addition, the mixing state of PM<sub>1</sub> nonvolatile cations with SO<sub>4</sub><sup>2-</sup>, NO<sub>3</sub><sup>-</sup>, and NH<sub>4</sub><sup>+</sup> remains to be investigated (Guo et al., 2016, 2017). Previous studies showed that including the nonvolatile cations in ISORROPIA-II does not significantly affect the pH calculations unless the cations become important relative to anions (Guo et al., 2016; Song et al., 2018). The sensitivity test for Beijing winter conditions suggested that with nonvolatile cations, the predicted pH values increase by about 0.1 units.

In this study, the transition in aerosol composition was mainly reflected in the variations in nitrate and sulfate concentrations. For the analysis of the sensitivity of aerosol properties to particle composition, a selected sulfate concentration combined with the average temperature, RH, and total ammonia concentration (NH<sub>3</sub> + NH<sub>4</sub><sup>+</sup>) during the winters of 2014 and 2017 was input into the ISORROPIA-II model, where the total nitrate concentration (HNO<sub>3</sub> + NO<sub>3</sub><sup>-</sup>) was left as the free variable. The gaseous HNO<sub>3</sub> and

NH<sub>3</sub> concentrations were not directly measured during our campaign. But long-term measurements in Beijing showed that gaseous NH<sub>3</sub> concentration correlated well with NO<sub>x</sub> concentration in winter (Meng et al., 2011). Therefore, the empirical equation derived from Meng et al. (2011),  $\text{NH}_3 \text{ (ppb)} = 0.34 \times \text{NO}_x \text{ (ppb)} + 0.63$ , was applied to estimate the gaseous NH<sub>3</sub> concentration. On average, the NH<sub>3</sub> concentration was approximated to be 14.0  $\mu\text{g m}^{-3}$  during the winters of 2014 and 2017, consistent with previous observations in the same season of Beijing (Meng et al., 2011; Zhao et al., 2016; Zhang et al., 2018). The total nitrate concentration, including both gaseous HNO<sub>3</sub> and particulate nitrate, varied from 0.2 to 75  $\mu\text{g m}^{-3}$  for the sensitivity study.

## 3 Results and discussions

### 3.1 Overall variations in aerosol characteristics from 2014 to 2017

Figures S14 and S15 display the temporal variations in meteorological parameters, trace gases, and aerosol species during the two winter campaigns, with the average values shown in Table 1. Compared to the frequently occurring haze episodes in the winter of 2014, more clean days with lower PM<sub>1</sub> concentrations were observed in the winter of 2017. On average, the PM<sub>1</sub> concentrations were 66.2  $\mu\text{g m}^{-3}$  and 33.4  $\mu\text{g m}^{-3}$  during the winters of 2014 and 2017, respectively. The large reduction in PM<sub>1</sub> concentration reflects the effectiveness of pollution abatement strategies. Satellite-derived estimates also showed an evident decrease in PM<sub>2.5</sub> concentration in North China in recent years (Gui et al., 2019).

#### 3.1.1 Changes in SIA characteristics

Sulfate, nitrate, and ammonium are the dominant components in SIAs and are generally recognized as ammonium sulfate and ammonium nitrate in PM<sub>2.5</sub>. With the implementation of clean air actions, sulfate underwent the largest decline in the mass concentration among all SIA species (from 7.7  $\mu\text{g m}^{-3}$  to 2.8  $\mu\text{g m}^{-3}$  during 2014-2017). The decreases in particulate nitrate and ammonium during this period were 1.3  $\mu\text{g m}^{-3}$  and 1.5  $\mu\text{g m}^{-3}$ , respectively. Different changes in the mass concentration of SIA species led to variations in the PM<sub>1</sub> chemical composition. As illustrated in Fig. 1, nitrate exhibited an increasing mass fraction in PM<sub>1</sub> from 18% to 30%, whereas the mass contribution of sulfate decreased from 12% to 8%. Correspondingly, the mass ratio of nitrate/sulfate increased from 1.4 in 2014 to 3.5 in 2017. Based on the measurements in Beijing from November to December, Xu et al. (2019) also observed a higher nitrate/sulfate ratio in 2016 (1.36) than in 2014 (0.72). Similar annual variations in aerosol chemical composition were found in North America over 2000-2016, with an increased proportion of nitrate and a decreased contribution of sulfate (van Donkelaar et al., 2019). The diurnal cycles of SIAs are displayed in Fig. 2. All SIA species showed similar diel trends in the two winters, with increasing concentrations after noon due to enhanced photochemical processes and peak concentrations at night caused by a lower boundary layer height. The CO-scaled diurnal plots for SIA species are shown in Fig. S16 to eliminate the influence of different dilution/mixing conditions. However, the absolute variations in the SIA mass concentration differed greatly between 2014 and 2017. While the mass concentration of sulfate decreased by a factor of 2-3 in 2017, nitrate and ammonium showed much smaller reductions of 15-40% in their mass concentrations throughout the day. Previous studies have concluded that the dramatically enhanced contribution of sulfate was a main driving factor of winter haze pollution in China (Wang et al., 2014; Wang et al., 2016; H. Y. Li et al., 2017). However, with the emission mitigation efforts, the role of SIA species in aerosol pollution changed significantly. Aerosol pollution was classified into three categories in this study: clean ( $\text{PM}_{10} \leq 35 \mu\text{g m}^{-3}$ ), slightly polluted ( $35 < \text{PM}_{10} \leq 115 \mu\text{g m}^{-3}$ ), and polluted ( $\text{PM}_{10} > 115 \mu\text{g m}^{-3}$ ). The contributions of different pollution levels and the PM<sub>10</sub> chemical compositions at each pollution level are shown in Fig. 3 for the winters of 2014 and 2017. While the polluted level accounted for 38% of the observation period in the winter of 2014, only 14% of the observation period was recognized as being polluted in the winter of 2017. In 2014, the mass fraction of sulfate in PM<sub>10</sub> was 16.1% during clean

230 periods. With the increase in pollution level, the contribution of sulfate increased from 10.6% in slightly polluted periods to 13.6%  
231 in polluted periods, while the mass fraction of nitrate decreased. In contrast, sulfate comprised a smaller fraction of haze  
232 development in 2017 compared to 2014. It was nitrate that exhibited a substantially increased mass fraction at higher PM<sub>1</sub> loadings  
233 in the winter of 2017. From clean to polluted periods, the nitrate contribution to PM<sub>1</sub> increased from 22.6% to 34.9%. These results  
234 demonstrated that aerosol pollution in Beijing has gradually changed from sulfate-driven to nitrate-driven in recent years.

### 235 3.1.2 Changes in OA characteristics

236 In response to the strict emission controls, the mass concentration of organics declined by ~18.5  $\mu\text{g m}^{-3}$  from 2014 (30.4  $\mu\text{g m}^{-3}$ )  
237 to 2017 (11.9  $\mu\text{g m}^{-3}$ ), which was mainly caused by OOA (~6.8  $\mu\text{g m}^{-3}$ ) and CCOA (~6.0  $\mu\text{g m}^{-3}$ ). The decrease in the mass  
238 concentration of HOA was 2.6  $\mu\text{g m}^{-3}$ , which was associated with the strengthened controls on vehicle emissions. BBOA decreased  
239 by 3.2  $\mu\text{g m}^{-3}$  because the use of traditional biofuels, such as wood and crop residuals, was forbidden in Beijing by the end of 2016.  
240 Generally, the concentrations of all OA factors declined substantially throughout the day in 2017. For primary factors, the  
241 reductions in their mass concentrations were much higher at night than during the day (Fig. 2). Compared to 2014, CCOA decreased  
242 by a factor of 4-5 at night in 2017 and a factor of 1.5 during the day.

243 Overall, the mass fraction of organics in PM<sub>1</sub> declined from 49% to 36% over the period (Fig. 1). The source apportionment results  
244 demonstrated that coal combustion was largely accountable for the reduced contribution of organics. During 2014-2017, the mass  
245 fraction of CCOA in the total OA decreased from 27% to 18%. Reports from the Beijing Municipal Environmental Protection  
246 Bureau (MEPB) also revealed that the contribution of coal combustion to aerosol pollution showed a large decrease during 2013-  
247 2017. The decline in CCOA was largely driven by the reduced emissions of organics from coal combustion with the implementation  
248 of clean air actions. In contrast, the mass contribution of OOA in the total OA increased from 41% to 49% during 2014-2017.  
249 OOA is formed in the atmosphere through various oxidation reactions of volatile organic compounds (VOCs). From 2013 to 2017,  
250 VOCs emissions decreased by approximately half in Beijing but remained constant in the surrounding regions. Large amounts of  
251 OOA brought to Beijing via regional transport weakened the efforts of local emission cuts. Therefore, stronger emission controls  
252 of VOCs need to be placed in both local Beijing and adjacent areas in the future.

## 253 3.2 Factors affecting aerosol characteristics from 2014 to 2017

### 254 3.2.1 Meteorological conditions

255 To evaluate the influence of weather conditions on air quality improvement, we compared the daily changes in meteorological  
256 parameters during the winters of 2014 and 2017 (Fig. S17). Compared to 2014, the temperature in 2017 was slightly lower  
257 throughout the whole day, which may have facilitated gas-particle conversion for semivolatile species, such as ammonium nitrate.  
258 Although the RH was similar between 2014 and 2017 during the daytime, the nighttime RH in 2017 was slightly higher than that  
259 in 2014, which was favorable for the heterogeneous reactions of secondary species. On average, the observed RH was 29.6% in  
260 the winter of 2014 and 33.9% in the winter of 2017. Diurnal cycles of WS showed that the WS in winter of 2017 was somewhat  
261 higher, implying beneficial conditions for the dispersal of air pollutants. To illustrate the variations in WD, the observed data were  
262 classified into four groups: from north to east (N-E;  $0^\circ \leq \text{WD} < 90^\circ$ ), east to south (E-S;  $90^\circ \leq \text{WD} < 180^\circ$ ), south to west (S-W;  
263  $180^\circ \leq \text{WD} < 270^\circ$ ), and west to north (W-N;  $270^\circ \leq \text{WD} \leq 360^\circ$ ). As displayed in Fig. S17d, the winters of 2014 and 2017 were  
264 both dominated by W-N and N-E, which usually bring clean air masses. After noon, the contribution of winds from S-W started  
265 to increase. According to previous studies, southerly winds arriving in Beijing generally carry higher levels of air pollutants from  
266 the southern regions (Sun et al., 2006; Zhao et al., 2009).

Simulations with the WRF-CMAQ model helped to assess the relative importance of meteorology for changes in aerosol concentration and chemical composition. The effects of meteorology were quantified by comparing cases *A* and *C* or cases *B* and *D*. The differences between *A* and *D* or *B* and *C* reflected the effectiveness of emission control. For the total PM<sub>2.5</sub> concentration, the simulation results clearly demonstrated that variations in meteorology from 2014 to 2017 had a much lower influence on the PM<sub>2.5</sub> reduction than the changes in air pollutant emissions (Fig. S18). On average, changes in weather conditions resulted in a PM<sub>2.5</sub> decrease of 9.6 µg m<sup>-3</sup>, which explained 24.8% of the total PM<sub>2.5</sub> reduction. These results suggest that meteorological variations are far from sufficient to explain PM<sub>2.5</sub> abatement during 2014-2017. In terms of aerosol composition, we compared the simulated results of cases *B* and *D* and found that meteorological changes from 2014 to 2017 had a negligible influence on the chemical composition of PM<sub>2.5</sub> (Fig. 4). Therefore, we conclude that weather conditions in 2017 marginally favored air quality improvement in Beijing, and emission reductions in air pollutants played a dominant role in the variations in aerosol concentration and composition.

### 3.2.2 Emission changes

According to both the observations (Fig. 1) and simulation results (Fig. 5a), sulfate and organics experienced the largest decreases among different components in Beijing from 2014 to 2017, which is consistent with the considerable emission reductions in SO<sub>2</sub> and primary OC in local Beijing and its surrounding regions (Fig. 6; i.e., Tianjin, Hebei, Shandong, Henan, Shanxi, and Inner Mongolia). Comparatively, the wintertime nitrate concentration showed the lowest reduction during 2014-2017, which was expected from the smaller emission cut of NO<sub>x</sub> in Beijing and its surrounding areas.

Based on the bottom-up emission inventories (Zheng et al., 2018; Cheng et al., 2019), SO<sub>2</sub> emissions decreased by 79.9% in Beijing during 2014-2017, mainly due to the effective control of coal combustion sources and the optimization of the energy structure. By the end of 2017, all coal-fired power units were shut down, and small coal-fired boilers with capacities of <7 MW were eliminated in Beijing, which reduced coal use by more than 17 million tons. In addition, most of the clustered and highly polluted enterprises and factories were phased out during this period. These control measures remarkably reduced SO<sub>2</sub> emissions from power and industry sectors. Enhanced energy restructuring was also implemented in the residential sector. During 2013-2017, more than 2 million tons of residential coal was replaced by cleaner natural gas and electricity, involving 900,000 households in Beijing. Apart from coal burning, the use of traditional biomass, such as wood and crops, was thoroughly forbidden in Beijing by the end of 2016. The strict governance of residential fuel also made substantial contributions to the BC and OC emission reductions in Beijing, which decreased by 71.2% and 59.9%, respectively, during 2014-2017. In comparison, NO<sub>x</sub> showed a lower emission reduction of 38.1% from 2014 to 2017 in Beijing. The decline in NO<sub>x</sub> emissions was mainly caused by the strengthened emission control of on-road and off-road transportation, the shutdown of all coal-fired power plants, and the application of low-nitrogen-burning (LNB) technologies in industrial boilers. However, due to the insufficient end-of-pipe control of widespread gas-fired facilities and the rapid increase in the vehicle population (the number of vehicles in Beijing increased by nearly 10% during 2013-2017), the NO<sub>x</sub> emission reduction in Beijing was not as significant as the SO<sub>2</sub> emission reduction.

In adjacent regions, SO<sub>2</sub> emissions decreased by 50.6% from 2014 to 2017, while NO<sub>x</sub> emissions showed a much smaller reduction of 15.2%. Comparatively, the energy structure adjustments in surrounding areas were less intense than those in Beijing. Emission reductions in SO<sub>2</sub> and NO<sub>x</sub> in surrounding regions were mainly attributed to ultralow power plant emissions and the reinforced end-of-pipe control of key industries. Because of the looser emission standards for vehicles and the lack of vehicle management, control measures on transportation in adjacent regions were highly insufficient for NO<sub>x</sub> emission reduction compared with those in Beijing. Overall, the observed transition in PM<sub>1</sub> chemical composition with increasing nitrate contribution and decreasing sulfate fraction was in agreement with the emission changes in their precursors.



### 306 3.2.3 Regional transport

307 Variations in regional weather patterns and emission changes in air pollutants in surrounding regions influenced the effect of  
308 regional transport on aerosol characteristics in Beijing. Statistical analysis of air mass trajectories was performed using the  
309 HYSPLIT model. Based on the clustering technique, back trajectories were classified into groups of similar length and curvature  
310 to identify the main airflows affecting the site. The five-cluster solution and seven-cluster solution were adopted for the winters of  
311 2014 and 2017, respectively. The  $PM_{10}$  mass concentration and mass composition for each cluster are shown in Fig. S19. For a  
312 better comparison between 2014 and 2017, clusters were further grouped into two categories according to  $PM_{10}$  loadings. Clusters  
313 arriving in Beijing when the local  $PM_{10}$  concentration was less than  $35 \mu g m^{-3}$  were recognized as clean clusters, while clusters with  
314  $PM_{10}$  concentrations greater than  $35 \mu g m^{-3}$  were defined as polluted clusters. As displayed in Fig. 7, the average  $PM_{10}$  concentration  
315 in local Beijing was  $114 \mu g m^{-3}$  in 2014 when the polluted clusters arrived, which was much higher than that in 2017 ( $74 \mu g m^{-3}$ ).  
316 While the contribution of polluted clusters in 2014 was 47%, polluted air masses transported from surrounding regions influenced  
317 Beijing approximately 20% of the time in 2017. The results here indicate that compared to 2014, Beijing was less influenced by  
318 polluted air masses transported from surrounding areas in 2017 during the wintertime, which benefited air quality improvement.  
319 In addition, air masses in 2017 brought more nitrate and less sulfate to Beijing than those in 2014.  
320 The WRF-CMAQ model simulations showed that the contributions of regional transport to the  $PM_{2.5}$  concentration in Beijing were  
321  $31.4 \mu g m^{-3}$  and  $19.0 \mu g m^{-3}$  in the winters of 2014 and 2017, respectively (Fig. 5b). Although the proportion of regional transport  
322 (relative to the total  $PM_{2.5}$  concentration in Beijing) remained at approximately 35% in the two winters (34.4% in the winter of  
323 2014 and 36.4% in the winter of 2017), the absolute amount decreased by 39.6%. This result further supported that less  $PM_{2.5}$   
324 transported from surrounding regions indeed helped with  $PM_{2.5}$  abatement in Beijing. Compared with 2014, the variations in  $PM_{2.5}$   
325 components due to regional transport (Fig. 5b) in 2017 were basically consistent with the total aerosol composition changes that  
326 were observed (Fig. 1) and simulated (Fig. 5a) in Beijing. Sulfate had the most notable decrease, with a decrease of 57.9% in its  
327 mass concentration, and the regional transport of OM and BC decreased by over 38%. The significant reduction in sulfate was  
328 mainly attributed to the effective  $SO_2$  emission controls in the surrounding regions, such as the special emission limits for power  
329 plants and the innovation of industrial boilers. The decreasing rate of regional transport OM was obviously lower than the total  
330 change, suggesting that the local emission controls of VOCs and primary OM in Beijing had a dominant contribution to the decrease  
331 in OM. The reduction in nitrate from regional transport was much smaller than that in other components. This was not only due to  
332 the insufficient  $NO_x$  emission controls in the surrounding areas but also the relatively rich ammonium environment in North China,  
333 which might have weakened the effects of  $NO_x$  reductions. Therefore, the collaborative reductions in  $NO_x$  and  $NH_3$  are important  
334 for future air pollution control strategies (Liu et al., 2019).

### 335 3.2.4 Formation mechanisms

336 From a traditional viewpoint, sulfate formation mainly includes  $SO_2$  oxidation by OH in the gas phase and  $SO_2$  oxidation in cloud  
337 droplets by  $H_2O_2$  and  $O_3$  in the aqueous phase (Seinfeld and Pandis, 2012). This is actually the case for global sulfate production  
338 (Roelofs et al., 1998). The formation rate of sulfate through aqueous reactions is typically much faster than that through gas-phase  
339 oxidations. Recently, studies have found that  $SO_2$  oxidation by  $NO_2$  in aerosol water with near neutral aerosol acidity, which is  
340 usually ignored in current model simulations, plays an important role in the persistent formation of sulfate during haze events in  
341 northern China (B. Zheng et al., 2015; Cheng et al., 2016; Wang et al., 2016). Others pointed out that regardless of the high  $NH_3$   
342 levels, aerosols are always moderately acidic in northern China, and there are probably other alternative formation pathways  
343 contributing to fast sulfate production in haze pollution (Guo et al., 2017b; Liu et al., 2017; Song et al., 2018). As the  $SO_2$  emissions

decreased substantially with the clean air actions, the importance of heterogeneous chemistry in sulfate formation is highly uncertain.

To shed light on this query, the formation of sulfate with increasing RH was compared between 2014 and 2017 (Fig. 8). The sulfur oxidation ratio (SOR) was estimated as the molar ratio of sulfate to the sum of sulfate and SO<sub>2</sub> to quantify the degree of SO<sub>2</sub> oxidations (Zheng et al., 2015; Li et al., 2016). Median values were used for comparison between 2014 and 2017 to avoid bias caused by outliers. When the RH>50%, SOR started to increase significantly with the enhancement in RH in 2014, which was consistent with previous observations in Beijing in 2013 (G. J. Zheng et al., 2015). A year-long study in Beijing from 2012 to 2013 also revealed that a rapid increase in SOR was found at a RH threshold of ~45% (Fang et al., 2019). However, the starting point of SOR growth was clearly delayed in 2017, with a higher RH of 70%. Considering the decrease in the SO<sub>2</sub> mixing ratio from 15.5 ppb in the winter of 2014 to 2.8 ppb in the winter of 2017 (Table 1), we speculated that with the large reduction in gaseous precursors, the rapid formation of sulfate through heterogeneous reaction is more difficult to occur. In addition to emission reduction, reduced regional transport from southern polluted regions in 2017 helped to lower SO<sub>2</sub> concentrations in Beijing. Previous studies have revealed the positive feedback between aerosols and boundary layers, as high aerosol loadings could decrease the boundary layer height and further increase aerosol concentrations (Petäjä et al., 2016; Z. Li et al., 2017). With a lower PM<sub>2.5</sub> concentration in 2017, the interactions between aerosols and the boundary layer were weakened, which in turn also favored a decrease in the SO<sub>2</sub> concentration. At a lower RH, the SOR in 2017 (~0.14) was unexpectedly higher than that in 2014 (~0.06), demonstrating a higher sulfate production rate in 2017. Similar results have been observed over the eastern United States, where a considerable decrease in SO<sub>2</sub> resulted in the more efficient formation of particulate sulfate during wintertime (Shah et al., 2018). Combining airborne measurements, ground-based observations, and GEOS-Chem simulations, Shah et al. (2018) explained that sulfate production in winter is limited by the availability of oxidants and particle acidity. At lower concentrations of precursor gases, the oxidant limitation on SO<sub>2</sub> oxidation weakened, leading to a higher formation rate of sulfate.

### 3.3 Influence of the transition in aerosol characteristics on particle properties

According to thermodynamic calculations, various aerosol properties were affected by changes in aerosol characteristics associated with clean air actions. As shown in Fig. 9a, nitrate and sulfate play key roles in determining the AWC in PM<sub>2.5</sub>. The decreasing mass concentrations of nitrate and sulfate result in a lower AWC. Similar observations have been reported previously across northern China, revealing that nitrate and sulfate are dominant anthropogenic inorganic salts driving AWC (Wu et al., 2018). With the clean air actions enacted, the mass concentrations of nitrate and sulfate decreased during 2013-2017, leading to an average decline in AWC from 12.0 to 8.5 μg m<sup>-3</sup>. Data for the winter of 2013 were acquired from Sun et al. (2016). The reduced AWC further helped air quality improvement by lowering the ambient aerosol mass and enhancing visibility. Because aqueous-phase reactions contribute largely to sulfate formation in winter, the decrease in AWC decelerated the formation of sulfate. In addition, the lower AWC slowed down the uptake coefficient of N<sub>2</sub>O<sub>5</sub> for heterogeneous processing, thereby suppressing the formation of particulate nitrate.

Figure 9b displays the effects of nitrate and sulfate concentrations on particle acidity. Particle acidity is largely driven by the mass concentration of sulfate and is less sensitive to the variation in nitrate. Particle pH substantially decreases with increasing sulfate concentration. Ding et al. (2019) suggested that sulfate is one of the common driving factors influencing particle acidity in Beijing across all four seasons. In contrast, more particulate nitrate leads to a slightly higher pH by increasing the particle liquid water and diluting aqueous H<sup>+</sup> concentrations. Through the comparison of pH predictions among various locations worldwide, Guo et al. (2018) also found that a higher particle pH was generally associated with higher concentrations of nitrate. During 2013-2017, the average particle pH varied from 4.5 to 5.3, with a significant decrease in sulfate concentration. The pH values here agree reasonably

with previous ISORROPIA-II calculations, showing that fine particles are moderately acidic in northern China during wintertime (Guo et al., 2017a; Liu et al., 2017; Song et al., 2018; Ding et al., 2019). When  $\text{pH} > 5.0$ , aqueous-phase productions of sulfate are dominated by  $\text{SO}_2$  oxidation with  $\text{H}_2\text{O}_2$ ,  $\text{O}_3$ , and  $\text{NO}_2$  under haze conditions in Beijing (Cheng et al., 2016). The sulfate oxidation rates by  $\text{O}_3$  and  $\text{NO}_2$  increase with increasing particle  $\text{pH}$ . Therefore, a more neutral atmosphere would favor aqueous-phase sulfate formation in Beijing. Particle acidity also influences the gas-particle partitioning of nitrate. The rising particle  $\text{pH}$  would result in a higher fraction of particulate nitrate ( $\epsilon(\text{NO}_3^-) = \frac{[\text{NO}_3^-]}{[\text{HNO}_3] + [\text{NO}_3^-]}$ ) (Guo et al., 2016). Figure S20a displays the variation in  $\epsilon(\text{NO}_3^-)$  as a function of particle  $\text{pH}$  under typical Beijing winter conditions (temperature of approximately  $0^\circ\text{C}$ ). With a particle  $\text{pH}$  below 3,  $\epsilon(\text{NO}_3^-)$  increases sufficiently with the enhancement in particle  $\text{pH}$ . However, when the particle  $\text{pH}$  is larger than 3,  $\epsilon(\text{NO}_3^-)$  remains relatively stable (approaching 1), consistent with previous findings by Guo et al. (2018). From 2013 to 2017, with the particle  $\text{pH}$  remaining above 3 in Beijing, no clear change in  $\epsilon(\text{NO}_3^-)$  was observed (Fig. S20b). The variations in nitrate and sulfate concentrations also affected the gas-particle partitioning of total ammonium ( $\text{NH}_x = \text{NH}_3 + \text{NH}_4^+$ ). As expected, the decreased concentrations of nitrate and sulfate led to a reduction in the ammonium particle fraction ( $\epsilon(\text{NH}_4^+) = \text{NH}_4^+/\text{NH}_x$ ; Fig. 10). From 2013 to 2017,  $\epsilon(\text{NH}_4^+)$  in Beijing always stayed below 0.4, indicating that most ammonium existed in the gas phase. Therefore, a minor reduction in  $\text{NH}_x$  would not be sufficient for air quality improvement. Guo et al. (2018) revealed that for winter haze conditions in Beijing, an approximate 60% decrease in  $\text{NH}_x$  was required to achieve an effective reduction in  $\text{PM}_{2.5}$ . Due to the close linkage between ammonia emissions and agricultural activities, it may be difficult to attain substantial ammonia reduction in China.

#### 400 4 Conclusions

This study investigated the variations in aerosol characteristics in Beijing during the winters of 2014 and 2017 by combining the online measurements of aerosol chemical composition with a comprehensive model analysis of meteorological conditions, anthropogenic emissions, and regional transport. The average  $\text{PM}_1$  concentration decreased from  $66.2 \mu\text{g m}^{-3}$  in the winter of 2014 to  $33.4 \mu\text{g m}^{-3}$  in the winter of 2017, with decreasing concentrations of organics, sulfate, nitrate, and ammonium by  $18.5 \mu\text{g m}^{-3}$ ,  $4.9 \mu\text{g m}^{-3}$ ,  $1.3 \mu\text{g m}^{-3}$ , and  $1.5 \mu\text{g m}^{-3}$ , respectively. These changes reduced the mass fractions of organics and sulfate from 59% to 36% and from 13% to 9%, respectively, whereas increased the nitrate contribution from 19% to 32%. Consequently, the winter haze pollution changed from sulfate-driven to nitrate-driven in Beijing from 2014 to 2017, implicating the increasing role of nitrate in aerosol pollution.

The chemical transport model simulations suggest that the rapidly declining emissions in Beijing and its adjacent regions account for ~75% of  $\text{PM}_{2.5}$  abatement in Beijing, and the remaining portion can be explained by the favorable weather conditions in 2017. The faster reductions in  $\text{SO}_2$  emissions compared to  $\text{NO}_x$  emissions are in line with the decreased sulfate contribution and increased nitrate fraction in observed aerosols, and the model simulations with these emission estimates can reproduce the relative changes in aerosol composition. Regional transport contributed moderately to the variations in aerosol concentration and its chemical composition, with less polluted air masses transported from surrounding regions to Beijing in the winter of 2017. The air masses were observed to have brought more nitrate and less sulfate to Beijing. Furthermore, the fast  $\text{SO}_2$ -to-sulfate conversion through heterogeneous reactions was observed to increase promptly at a RH threshold of ~50% in 2014, while a higher RH of 70% was observed in 2017. Based on these ambient observations, the suppressed sulfate formation during wintertime was possibly caused by the considerable decrease in  $\text{SO}_2$  emissions.

Thermodynamic calculations showed that the decreased sulfate and nitrate concentrations in 2017 caused a lower AWC in  $\text{PM}_{2.5}$ , which further decreased the ambient aerosol mass and weakened the formation rates of sulfate and nitrate through aqueous-phase

reactions. Particle acidity displayed a decline during 2014–2017, mostly driven by the declining sulfate concentration. In turn, the more neutral ambient environment would favor the aqueous oxidation of sulfate in Beijing. Analysis of the ammonium particle fraction indicated that most ammonium in Beijing existed in the gas phase. Therefore, increased efforts are needed to achieve an effective reduction in particle ammonium in the future.

#### Author contributions

QZ and KH conceived the study. HL conducted the field measurements and carried out the data analysis. JC provided the emission data and performed the model simulations. BZ participated the data analysis. HL, JC and QZ wrote the paper with inputs from all coauthors.

#### Acknowledgements

This work was funded by the National Natural Science Foundation of China (41571130035, 41571130032 and 41625020).

#### References

- Bey, I., Jacob, D. J., Yantosca, R. M., Logan, J. A., Field, B. D., Fiore, A. M., Li, Q., Liu, H., Mickley, L. J., and Schultz, M. G.: Global modeling of tropospheric chemistry with assimilated meteorology: Model description and evaluation, *J. Geophys. Res.*, 106, D19, 23073–23095, <https://doi.org/10.1029/2001JD000807>, 2001.
- Canonaco, F., Crippa, M., Slowik, J. G., Baltensperger, U., and Prevot, A. S. H.: SoFi, an IGOR-based interface for the efficient use of the generalized multilinear engine (ME-2) for the source apportionment: ME-2 application to aerosol mass spectrometer data, *Atmos Meas Tech*, 6, 3649–3661, 2013.
- Cheng, J., Su, J., Cui, T., Li, X., Dong, X., Sun, F., Yang, Y., Tong, D., Zheng, Y., Li, Y., Li, J., Zhang, Q., and He, K.: Dominant role of emission reduction in PM<sub>2.5</sub> air quality improvement in Beijing during 2013–2017: a model-based decomposition analysis, *Atmos. Chem. Phys.*, 19, 6125–6146, <https://doi.org/10.5194/acp-19-6125-2019>, 2019.
- Cheng, Y. F., Zheng, G. J., Wei, C., Mu, Q., Zheng, B., Wang, Z. B., Gao, M., Zhang, Q., He, K. B., Carmichael, G., Poschl, U., and Su, H.: Reactive nitrogen chemistry in aerosol water as a source of sulfate during haze events in China, *Sci Adv*, 2, 2016.
- Cohen, A. J., Brauer, M., Burnett, R., Anderson, H. R., Frostad, J., Estep, K., Balakrishnan, K., Brunekreef, B., Dandona, L., Dandona, R., Feigin, V., Freedman, G., Hubbell, B., Jobling, A., Kan, H., Knibbs, L., Liu, Y., Martin, R., Morawska, L., Pope, C. A., Shin, H., Straif, K., Shaddick, G., Thomas, M., van Dingenen, R., van Donkelaar, A., Vos, T., Murray, C. J. L., and Forouzanfar, M. H.: Estimates and 25-year trends of the global burden of disease attributable to ambient air pollution: an analysis of data from the Global Burden of Diseases Study 2015, *Lancet*, 389, 1907–1918, 2017.
- Fang, Y., Ye, C., Wang, J., Wu, Y., Hu, M., Lin, W., Xu, F., and Zhu, T.: RH and O<sub>3</sub> concentration as two prerequisites for sulfate formation, *Atmos. Chem. Phys. Discuss.*, 2019, 1–25, [10.5194/acp-2019-284](https://doi.org/10.5194/acp-2019-284), 2019.
- Fountoukis, C., and Nenes, A.: ISORROPIA II: a computationally efficient thermodynamic equilibrium model for K<sup>+</sup>-Ca<sup>2+</sup>-Mg<sup>2+</sup>-NH<sub>4</sub><sup>+</sup>-Na<sup>+</sup>-SO<sub>4</sub><sup>2-</sup>-NO<sub>3</sub><sup>-</sup>-Cl-H<sub>2</sub>O aerosols, *Atmos Chem Phys*, 7, 4639–4659, 2007.
- Gao, M., Carmichael, G. R., Saide, P. E., Lu, Z., Yu, M., Streets, D. G., and Wang, Z.: Response of winter fine particulate matter concentrations to emission and meteorology changes in North China, *Atmos. Chem. Phys.*, 16, 11837–11851, [10.5194/acp-16-11837-2016](https://doi.org/10.5194/acp-16-11837-2016), 2016.
- Geng, G., Zhang, Q., Tong, D., Li, M., Zheng, Y., Wang, S., and He, K.: Chemical composition of ambient PM<sub>2.5</sub> over China and relationship to precursor emissions during 2005–2012, *Atmos. Chem. Phys.*, 17, 9187–9203, [10.5194/acp-17-9187-2017](https://doi.org/10.5194/acp-17-9187-2017), 2017.
- Gui, K., Che, H., Wang, Y., Wang, H., Zhang, L., Zhao, H., Zheng, Y., Sun, T., and Zhang, X.: Satellite-derived PM<sub>2.5</sub> concentration trends over Eastern China from 1998 to 2016: Relationships to emissions and meteorological parameters, *Environ Pollut*, 247, 1125–1133, <https://doi.org/10.1016/j.envpol.2019.01.056>, 2019.

461 Guo, H., Xu, L., Bougiatioti, A., Cerully, K. M., Capps, S. L., Hite, J. R., Carlton, A. G., Lee, S. H., Bergin, M. H., Ng, N. L.,  
 462 Nenes, A., and Weber, R. J.: Fine-particle water and pH in the southeastern United States, *Atmos Chem Phys*, 15, 5211-5228,  
 463 2015.

464 Guo, H., Sullivan, A. P., Campuzano-Jost, P., Schroder, J. C., Lopez-Hilfiker, F. D., Dibb, J. E., Jimenez, J. L., Thornton, J. A.,  
 465 Brown, S. S., Nenes, A., and Weber, R. J.: Fine particle pH and the partitioning of nitric acid during winter in the northeastern  
 466 United States, *Journal of Geophysical Research: Atmospheres*, 121, 10,355-310,376, 10.1002/2016JD025311, 2016.

467 Guo, H., Liu, J., Froyd, K. D., Roberts, J. M., Veres, P. R., Hayes, P. L., Jimenez, J. L., Nenes, A., and Weber, R. J.: Fine particle  
 468 pH and gas-particle phase partitioning of inorganic species in Pasadena, California, during the 2010 CalNex campaign, *Atmos.*  
 469 *Chem. Phys.*, 17, 5703-5719, 10.5194/acp-17-5703-2017, 2017a.

470 Guo, H., Weber, R. J., and Nenes, A.: High levels of ammonia do not raise fine particle pH sufficiently to yield nitrogen oxide-  
 471 dominated sulfate production, *Scientific Reports*, 7, 12109, 10.1038/s41598-017-11704-0, 2017a.

472 Guo, H. Y., Otjes, R., Schlag, P., Kiendler-Scharr, A., Nenes, A., and Weber, R. J.: Effectiveness of ammonia reduction on control  
 473 of fine particle nitrate, *Atmos Chem Phys*, 18, 12241-12256, 2018.

474 Hennigan, C. J., Izumi, J., Sullivan, A. P., Weber, R. J., and Nenes, A.: A critical evaluation of proxy methods used to estimate the  
 475 acidity of atmospheric particles, *Atmos. Chem. Phys.*, 15, 2775-2790, <https://doi.org/10.5194/acp-15-2775-2015>, 2015.

476 Huang, X. F., He, L. Y., Hu, M., Canagaratna, M. R., Sun, Y., Zhang, Q., Zhu, T., Xue, L., Zeng, L. W., Liu, X. G., Zhang, Y. H.,  
 477 Jayne, J. T., Ng, N. L., and Worsnop, D. R.: Highly time-resolved chemical characterization of atmospheric submicron  
 478 particles during 2008 Beijing Olympic Games using an Aerodyne High-Resolution Aerosol Mass Spectrometer, *Atmos Chem*  
 479 *Phys*, 10, 8933-8945, 2010.

480 Intergovernmental Panel on Climate Change (IPCC) (2013), *Climate Change 2013: The Physical Science Basis. Contribution of*  
 481 *Working Group I to the Fifth Assessment Report of the Intergovernmental Panel on Climate Change*, 1535 pp., Cambridge  
 482 Univ. Press, Cambridge, U. K., and New York.

483 Li, H. Y., Zhang, Q., Zhang, Q., Chen, C. R., Wang, L. T., Wei, Z., Zhou, S., Parworth, C., Zheng, B., Canonaco, F., Prevot, A. S.  
 484 H., Chen, P., Zhang, H. L., Wallington, T. J., and He, K. B.: Wintertime aerosol chemistry and haze evolution in an extremely  
 485 polluted city of the North China Plain: significant contribution from coal and biomass combustion, *Atmos Chem Phys*, 17,  
 486 4751-4768, 2017.

487 Li, H. Y., Zhang, Q., Zheng, B., Chen, C. R., Wu, N. N., Guo, H. Y., Zhang, Y. X., Zheng, Y. X., Li, X., and He, K. B.: Nitrate-  
 488 driven urban haze pollution during summertime over the North China Plain, *Atmos Chem Phys*, 18, 5293-5306, 2018.

489 Li, M., Zhang, Q., Kurokawa, J. I., Woo, J. H., He, K., Lu, Z., Ohara, T., Song, Y., Streets, D. G., Carmichael, G. R., Cheng, Y.,  
 490 Hong, C., Huo, H., Jiang, X., Kang, S., Liu, F., Su, H., and Zheng, B.: MIX: a mosaic Asian anthropogenic emission inventory  
 491 under the international collaboration framework of the MICS-Asia and HTAP, *Atmos. Chem. Phys.*, 17, 935-963,  
 492 <https://doi.org/10.5194/acp-17-935-2017>, 2017.

493 Li, T.-C., Yuan, C.-S., Huang, H.-C., Lee, C.-L., Wu, S.-P., and Tong, C.: Inter-comparison of Seasonal Variation, Chemical  
 494 Characteristics, and Source Identification of Atmospheric Fine Particles on Both Sides of the Taiwan Strait, *Scientific Reports*,  
 495 6, 22956, 10.1038/srep22956 <https://www.nature.com/articles/srep22956#supplementary-information>, 2016.

496 Li, Z., Guo, J., Ding, A., Liao, H., Liu, J., Sun, Y., Wang, T., Xue, H., Zhang, H., and Zhu, B.: Aerosol and boundary-layer  
 497 interactions and impact on air quality, *National Science Review*, 4, 810-833, 10.1093/nsr/nwx117 %J National Science  
 498 Review, 2017.

499 Liang, P. F., Zhu, T., Fang, Y. H., Li, Y. R., Han, Y. Q., Wu, Y. S., Hu, M., and Wang, J. X.: The role of meteorological conditions  
 500 and pollution control strategies in reducing air pollution in Beijing during APEC 2014 and Victory Parade 2015, *Atmos Chem*  
 501 *Phys*, 17, 2017.

502 Liu, M. M., Bi, J., and Ma, Z. W.: Visibility-Based PM<sub>2.5</sub> Concentrations in China: 1957-1964 and 1973-2014, *Environmental*  
 503 *Science & Technology*, 51, 13161-13169, 2017.

504 Liu, M. X., Song, Y., Zhou, T., Xu, Z. Y., Yan, C. Q., Zheng, M., Wu, Z. J., Hu, M., Wu, Y. S., and Zhu, T.: Fine particle pH  
 505 during severe haze episodes in northern China, *Geophys Res Lett*, 44, 5213-5221, 2017.

506 Liu, M. X., Huang, X., Song, Y., Tang, J., Cao, J., Zhang, X., Zhang, Q., Wang, S., Xu, T., Kang, L., Cai, X., Zhang, H., Yang, F.,  
 507 Wang, H., Yu, J., Lau, Alexis K. H., He, L., Huang, X., Duan, L., Ding A., Xue, L., Gao, J., Liu, B., and Zhu, T.: Ammonia  
 508 emission control in China would mitigate haze pollution and nitrogen deposition, but worsen acid rain, *PANS*, 116 (16) 7760-  
 509 7765, <https://doi.org/10.1073/pnas.1814880116>, 2019.

510 Meng, Z. Y., Lin, W. L., Jiang, X. M., Yan, P., Wang, Y., Zhang, Y. M., Jia, X. F., and Yu, X. L.: Characteristics of atmospheric  
 511 ammonia over Beijing, China, *Atmos. Chem. Phys.*, 11, 6139-6151, <https://doi.org/10.5194/acp-11-6139-2011>, 2011.

512 Middlebrook, A. M., Bahreini, R., Jimenez, J. L., and Canagaratna, M. R.: Evaluation of Composition-Dependent Collection  
 513 Efficiencies for the Aerodyne Aerosol Mass Spectrometer using Field Data, *Aerosol Sci Tech*, 46, 258-271, 2012. Ng, N. L.,  
 514 Herndon, S. C., Trimborn, A., Canagaratna, M. R., Croteau, P. L., Onasch, T. B., Sueper, D., Worsnop, D. R., Zhang, Q., Sun,  
 515 Y. L., and Jayne, J. T.: An Aerosol Chemical Speciation Monitor (ACSM) for Routine Monitoring of the Composition and  
 516 Mass Concentrations of Ambient Aerosol, *Aerosol Sci Tech*, 45, 780-794, 2011a.

517 Ng, N. L., Canagaratna, M. R., Jimenez, J. L., Zhang, Q., Ulbrich, I. M., and Worsnop, D. R.: Real-Time Methods for Estimating  
 518 Organic Component Mass Concentrations from Aerosol Mass Spectrometer Data, *Environmental Science & Technology*, 45,  
 519 910-916, 2011b.

520 Paatero, P.: The multilinear engine - A table-driven, least squares program for solving multilinear problems, including the n-way  
 521 parallel factor analysis model, *J Comput Graph Stat*, 8, 854-888, 1999.

522 Petäjä, T., Järvi, L., Kerminen, V. M., Ding, A. J., Sun, J. N., Nie, W., Kujansuu, J., Virkkula, A., Yang, X., Fu, C. B., Zilitinkevich,  
 523 S., and Kulmala, M.: Enhanced air pollution via aerosol-boundary layer feedback in China, *Scientific Reports*, 6, 18998,  
 524 10.1038/srep18998 <https://www.nature.com/articles/srep18998#supplementary-information>, 2016.

525 Petzold, A., and Schonlinner, M.: Multi-angle absorption photometry - a new method for the measurement of aerosol light  
 526 absorption and atmospheric black carbon, *J Aerosol Sci*, 35, 421-441, 2004.

527 Pope, C. A., Ezzati, M., and Dockery, D. W.: Fine-Particulate Air Pollution and Life Expectancy in the United States., *New Engl*  
 528 *J Med*, 360, 376-386, 2009.

529 Pui, D. Y. H., Chen, S. C., and Zuo, Z. L.: PM<sub>2.5</sub> in China: Measurements, sources, visibility and health effects, and mitigation,  
 530 *Particuology*, 13, 1-26, 2014.

531 Roelofs, G.-J. A. N., Lelieveld, J. O. S., and Ganzeveld, L.: Simulation of global sulfate distribution and the influence on effective  
 532 cloud drop radii with a coupled photochemistry sulfur cycle model, *Tellus B*, 50, 224-242, 10.1034/j.1600-0889.1998.t01-2-  
 533 00002.x, 1998.

534 Seinfeld, J. H. and Pandis, S. N.: *Atmospheric chemistry and physics: from air pollution to climate change*, 2nd Edition, John  
 535 Wiley & Sons, New York, USA, 2012.

536 Shah, V., Jaegle, L., Thornton, J. A., Lopez-Hilfiker, F. D., Lee, B. H., Schroder, J. C., Campuzano-Jost, P., Jimenez, J. L., Guo,  
 537 H. Y., Sullivan, A. P., Weber, R. J., Green, J. R., Fiddler, M. N., Bililign, S., Campos, T. L., Stell, M., Weinheimer, A. J.,  
 538 Montzka, D. D., and Brown, S. S.: Chemical feedbacks weaken the wintertime response of particulate sulfate and nitrate to  
 539 emissions reductions over the eastern United States, *P Natl Acad Sci USA*, 115, 8110-8115, 2018.

540 Song, S., Gao, M., Xu, W., Shao, J., Shi, G., Wang, S., Wang, Y., Sun, Y., and McElroy, M. B.: Fine-particle pH for Beijing winter  
 541 haze as inferred from different thermodynamic equilibrium models, *Atmos. Chem. Phys.*, 18, 7423-7438, 10.5194/acp-18-  
 542 7423-2018, 2018.

543 Squizzato, S., Masiol, M., Brunelli, A., Pistollato, S., Tarabotti, E., Rampazzo, G., and Pavoni, B.: Factors determining the  
 544 formation of secondary inorganic aerosol: a case study in the Po Valley (Italy), *Atmos Chem Phys*, 13, 1927-1939, 2013.

545 Su, X., Tie, X. X., Li, G. H., Cao, J. J., Huang, R. J., Feng, T., Long, X., and Xu, R. G.: Effect of hydrolysis of N<sub>2</sub>O<sub>5</sub> on nitrate  
 546 and ammonium formation in Beijing China: WRF-Chem model simulation, *Sci Total Environ*, 579, 221-229, 2017.

547 Sun, J., Liang, M., Shi, Z., Shen, F., Li, J., Huang, L., Ge, X., Chen, Q., Sun, Y., Zhang, Y., Chang, Y., Ji, D., Ying, Q., Zhang,  
 548 H., Kota, S. H., and Hu, J.: Investigating the PM<sub>2.5</sub> mass concentration growth processes during 2013–2016 in Beijing and  
 549 Shanghai, *Chemosphere*, 221, 452-463, <https://doi.org/10.1016/j.chemosphere.2018.12.200>, 2019.

550 Sun, K., Qu, Y., Wu, Q., Han, T., Gu, J., Zhao, J., Sun, Y., Jiang, Q., Gao, Z., Hu, M., Zhang, Y., Lu, K., Nordmann, S., Cheng,  
 551 Y., Hou, L., Ge, H., Furuuchi, M., Hata, M., and Liu, X.: Chemical characteristics of size-resolved aerosols in winter in  
 552 Beijing, *Journal of Environmental Sciences*, 26, 1641-1650, <https://doi.org/10.1016/j.jes.2014.06.004>, 2014.

553 Sun, Y. L., Zhuang, G. S., Tang, A. H., Wang, Y., and An, Z. S.: Chemical characteristics of PM<sub>2.5</sub> and PM<sub>10</sub> in haze-fog episodes  
 554 in Beijing, *Environmental Science & Technology*, 40, 3148-3155, 10.1021/es051533g, 2006.

555 Sun, Y., Jiang, Q., Wang, Z., Fu, P., Li, J., Yang, T., and Yin, Y.: Investigation of the sources and evolution processes of severe  
 556 haze pollution in Beijing in January 2013, *Journal of Geophysical Research: Atmospheres*, 119, 4380-4398,  
 557 10.1002/2014JD021641, 2014.

558 Sun, Y. L., Wang, Z. F., Du, W., Zhang, Q., Wang, Q. Q., Fu, P. Q., Pan, X. L., Li, J., Jayne, J., and Worsnop, D. R.: Long-term  
559 real-time measurements of aerosol particle composition in Beijing, China: seasonal variations, meteorological effects, and  
560 source analysis, *Atmos. Chem. Phys.*, 15, 10149-10165, 10.5194/acp-15-10149-2015, 2015.

561 Sun, Y. L., Du, W., Fu, P. Q., Wang, Q. Q., Li, J., Ge, X. L., Zhang, Q., Zhu, C. M., Ren, L. J., Xu, W. Q., Zhao, J., Han, T. T.,  
562 Worsnop, D. R., and Wang, Z. F.: Primary and secondary aerosols in Beijing in winter: sources, variations and processes,  
563 *Atmos Chem Phys*, 16, 8309-8329, 2016.

564 Tang, I. N., and Munkelwitz, H. R.: Aerosol Phase-Transformation and Growth in the Atmosphere, *J Appl Meteorol*, 33, 791-796,  
565 1994.

566 Ulbrich, I. M., Canagaratna, M. R., Zhang, Q., Worsnop, D. R., and Jimenez, J. L.: Interpretation of organic components from  
567 Positive Matrix Factorization of aerosol mass spectrometric data, *Atmos Chem Phys*, 9, 2891-2918, 2009.

568 van Donkelaar, A., Martin, R. V., Li, C., and Burnett, R. T.: Regional Estimates of Chemical Composition of Fine Particulate  
569 Matter Using a Combined Geoscience-Statistical Method with Information from Satellites, Models, and Monitors,  
570 *Environmental Science & Technology*, 10.1021/acs.est.8b06392, 2019. Wang, G. H., Zhang, R. Y., Gomez, M. E., Yang, L.  
571 X., Zamora, M. L., Hu, M., Lin, Y., Peng, J. F., Guo, S., Meng, J. J., Li, J. J., Cheng, C. L., Hu, T. F., Ren, Y. Q., Wang, Y.  
572 S., Gao, J., Cao, J. J., An, Z. S., Zhou, W. J., Li, G. H., Wang, J. Y., Tian, P. F., Marrero-Ortiz, W., Secrest, J., Du, Z. F.,  
573 Zheng, J., Shang, D. J., Zeng, L. M., Shao, M., Wang, W. G., Huang, Y., Wang, Y., Zhu, Y. J., Li, Y. X., Hu, J. X., Pan, B.,  
574 Cai, L., Cheng, Y. T., Ji, Y. M., Zhang, F., Rosenfeld, D., Liss, P. S., Duce, R. A., Kolb, C. E., and Molina, M. J.: Persistent  
575 sulfate formation from London Fog to Chinese haze, *P Natl Acad Sci USA*, 113, 13630-13635, 2016.

576 Wang, X. Y., Wang, K. C., and Su, L. Y.: Contribution of Atmospheric Diffusion Conditions to the Recent Improvement in Air  
577 Quality in China, *Scientific Reports*, 6, 2016.

578 Wang, Y., Zhang, Q., Jiang, J., Zhou, W., Wang, B., He, K., Duan, F., Zhang, Q., Philip, S., and Xie, Y.: Enhanced sulfate formation  
579 during China's severe winter haze episode in January 2013 missing from current models, 119, 10,425-410,440,  
580 doi:10.1002/2013JD021426, 2014.

581 Weber, R. J., Guo, H. Y., Russell, A. G., and Nenes, A.: High aerosol acidity despite declining atmospheric sulfate concentrations  
582 over the past 15 years, *Nat Geosci*, 9, 282-+, 2016.

583 Wu, Z. J., Wang, Y., Tan, T. Y., Zhu, Y. S., Li, M. R., Shang, D. J., Wang, H. C., Lu, K. D., Guo, S., Zeng, L. M., and Zhang, Y.  
584 H.: Aerosol Liquid Water Driven by Anthropogenic Inorganic Salts: Implying Its Key Role in Haze Formation over the North  
585 China Plain, *Environ Sci Tech Let*, 5, 160-166, 2018.

586 Xu, W. Q., Sun, Y. L., Chen, C., Du, W., Han, T. T., Wang, Q. Q., Fu, P. Q., Wang, Z. F., Zhao, X. J., Zhou, L. B., Ji, D. S., Wang,  
587 P. C., and Worsnop, D. R.: Aerosol composition, oxidation properties, and sources in Beijing: results from the 2014 Asia-  
588 Pacific Economic Cooperation summit study, *Atmos. Chem. Phys.*, 15, 13681-13698, 10.5194/acp-15-13681-2015, 2015.

589 Xu, W., Sun, Y., Wang, Q., Zhao, J., Wang, J., Ge, X., Xie, C., Zhou, W., Du, W., Li, J., Fu, P., Wang, Z., Worsnop, D. R., and  
590 Coe, H.: Changes in Aerosol Chemistry From 2014 to 2016 in Winter in Beijing: Insights From High-Resolution Aerosol  
591 Mass Spectrometry, *Journal of Geophysical Research: Atmospheres*, 124, 1132-1147, 10.1029/2018JD029245, 2019.

592 Yun, H., Wang, W. H., Wang, T., Xia, M., Yu, C., Wang, Z., Poon, S. C. N., Yue, D. L., and Zhou, Y.: Nitrate formation from  
593 heterogeneous uptake of dinitrogen pentoxide during a severe winter haze in southern China, *Atmos Chem Phys*, 18, 17515-  
594 17527, 2018.

595 Zhang, Q., Jimenez, J. L., Canagaratna, M. R., Ulbrich, I. M., Ng, N. L., Worsnop, D. R., and Sun, Y. L.: Understanding  
596 atmospheric organic aerosols via factor analysis of aerosol mass spectrometry: a review, *Anal Bioanal Chem*, 401, 3045-3067,  
597 2011.

598 Zhang, Y., Tang, A., Wang, D., Wang, Q., Benedict, K., Zhang, L., Liu, D., Li, Y., Collett Jr., J. L., Sun, Y., and Liu, X.: The  
599 vertical variability of ammonia in urban Beijing, China, *Atmos. Chem. Phys.*, 18, 16385-16398, [https://doi.org/10.5194/acp-](https://doi.org/10.5194/acp-18-16385-2018)  
600 18-16385-2018, 2018.

601 Zhao, M., Wang, S., Tan, J., Hua, Y., Wu, D., and Hao, J.: Variation of Urban Atmospheric Ammonia Pollution and its Relation  
602 with PM<sub>2.5</sub> Chemical Property in Winter of Beijing, China, *Aerosol Air Qual Res*, 16, 1378-1389, 10.4209/aaqr.2015.12.0699,  
603 2016.

604 Zhao, P., Chen, Y., and Su, J.: Size-resolved carbonaceous components and water-soluble ions measurements of ambient aerosol  
605 in Beijing, *Journal of Environmental Sciences*, 54, 298-313, <https://doi.org/10.1016/j.jes.2016.08.027>, 2017.

606 Zhao, X. J., Zhang, X. L., Xu, X. F., Xu, J., Meng, W., and Pu, W. W.: Seasonal and diurnal variations of ambient PM<sub>2.5</sub>  
 607 concentration in urban and rural environments in Beijing, *Atmos Environ*, 43, 2893-2900, 10.1016/j.atmosenv.2009.03.009,  
 608 2009.

609 Zheng, B., Zhang, Q., Zhang, Y., He, K. B., Wang, K., Zheng, G. J., Duan, F. K., Ma, Y. L., and Kimoto, T.: Heterogeneous  
 610 chemistry: a mechanism missing in current models to explain secondary inorganic aerosol formation during the January 2013  
 611 haze episode in North China, *Atmos Chem Phys*, 15, 2031-2049, 2015.

612 Zheng, B., Tong, D., Li, M., Liu, F., Hong, C., Geng, G., Li, H., Li, X., Peng, L., Qi, J., Yan, L., Zhang, Y., Zhao, H., Zheng, Y.,  
 613 He, K., and Zhang, Q.: Trends in China's anthropogenic emissions since 2010 as the consequence of clean air actions, *Atmos.*  
 614 *Chem. Phys.*, 18, 14095-14111, <https://doi.org/10.5194/acp-18-14095-2018>, 2018.

615 Zheng, J., Hu, M., Peng, J. F., Wu, Z. J., Kumar, P., Li, M. R., Wang, Y. J., and Guo, S.: Spatial distributions and chemical  
 616 properties of PM<sub>2.5</sub> based on 21 field campaigns at 17 sites in China, *Chemosphere*, 159, 480-487, 2016.

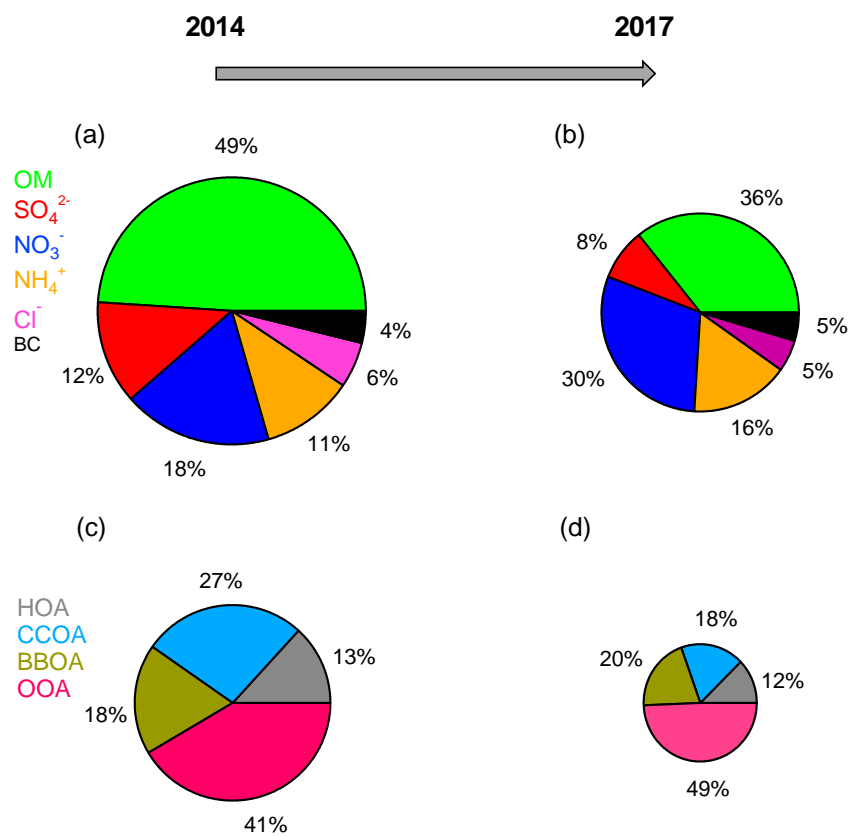
617 Zheng, G. J., Duan, F. K., Su, H., Ma, Y. L., Cheng, Y., Zheng, B., Zhang, Q., Huang, T., Kimoto, T., Chang, D., Poschl, U.,  
 618 Cheng, Y. F., and He, K. B.: Exploring the severe winter haze in Beijing: the impact of synoptic weather, regional transport  
 619 and heterogeneous reactions, *Atmos Chem Phys*, 15, 2969-2983, 2015.



620 **Table 1** Summary of the average meteorological parameters, mixing ratios of gaseous species, and mass concentrations of the PM<sub>1</sub> chemical  
621 components observed during the winters of 2014 and 2017.

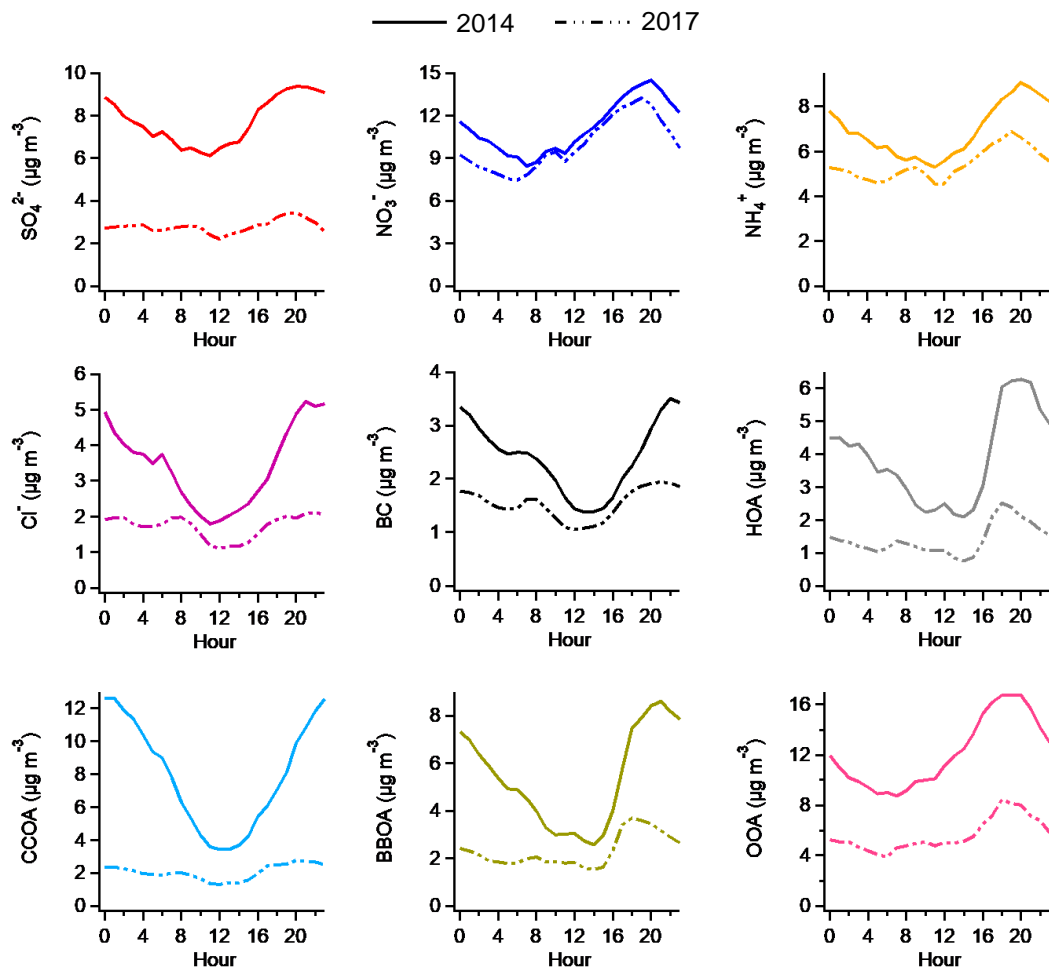
Sampling period		2014 winter	2017 winter
Meteorological parameters	T (°C)	1.70	-2.26
	RH (%)	29.6	33.9
	WS (m s <sup>-1</sup> )	1.58	1.73
Gaseous species	SO <sub>2</sub> (ppb)	15.5	2.8
	NO <sub>2</sub> (ppb)	26.0	24.9
	CO (ppm)	1.6	0.7
	O <sub>3</sub> (ppb)	14.4	15.5
Aerosol species (µg m <sup>-3</sup> )	Org	30.4	11.9
	HOA	4.1	1.5
	BBOA	5.6	2.4
	CCOA	8.2	2.2
	OOA	12.6	5.8
	SO <sub>4</sub> <sup>2-</sup>	7.8	2.8
	NO <sub>3</sub> <sup>-</sup>	11.2	9.9
	NH <sub>4</sub> <sup>+</sup>	6.9	5.4
	Cl <sup>-</sup>	3.4	1.7
	BC	2.4	1.5
	PM <sub>1</sub>	66.2	33.4

622



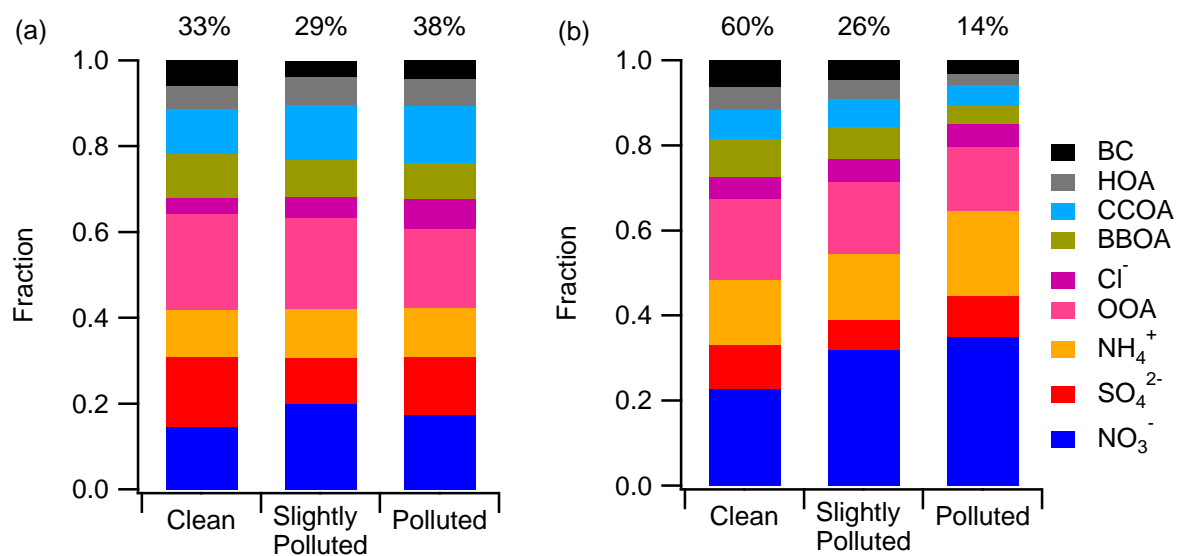
623

624 **Figure 1. Average chemical compositions of PM<sub>1</sub> and OA in (a, c) winter of 2014 and (b, d) winter of 2017. The decreases in the mass**  
 625 **concentrations of different components from 2014 to 2017 are as follows: 60.9% for organics, 64.1% for sulfate, 11.6% for nitrate, 21.7%**  
 626 **for ammonium, 50.0% for chloride, and 37.5% for BC.**



627

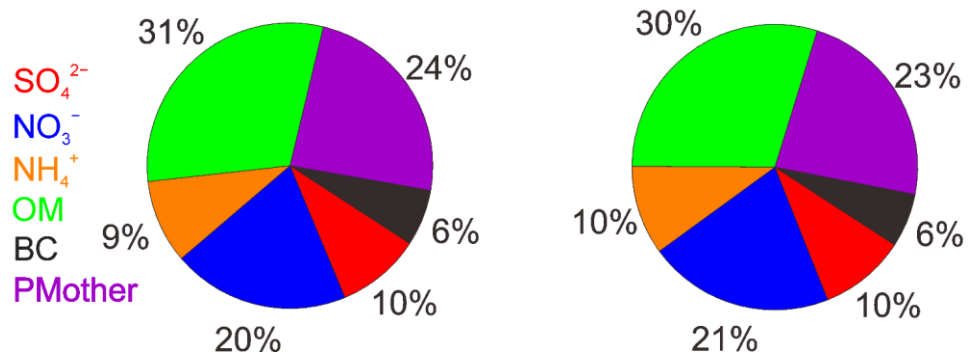
628 Figure 2. Average diurnal cycles of different aerosol species in the winter of 2014 (solid line) and winter of 2017 (dashed line).



629

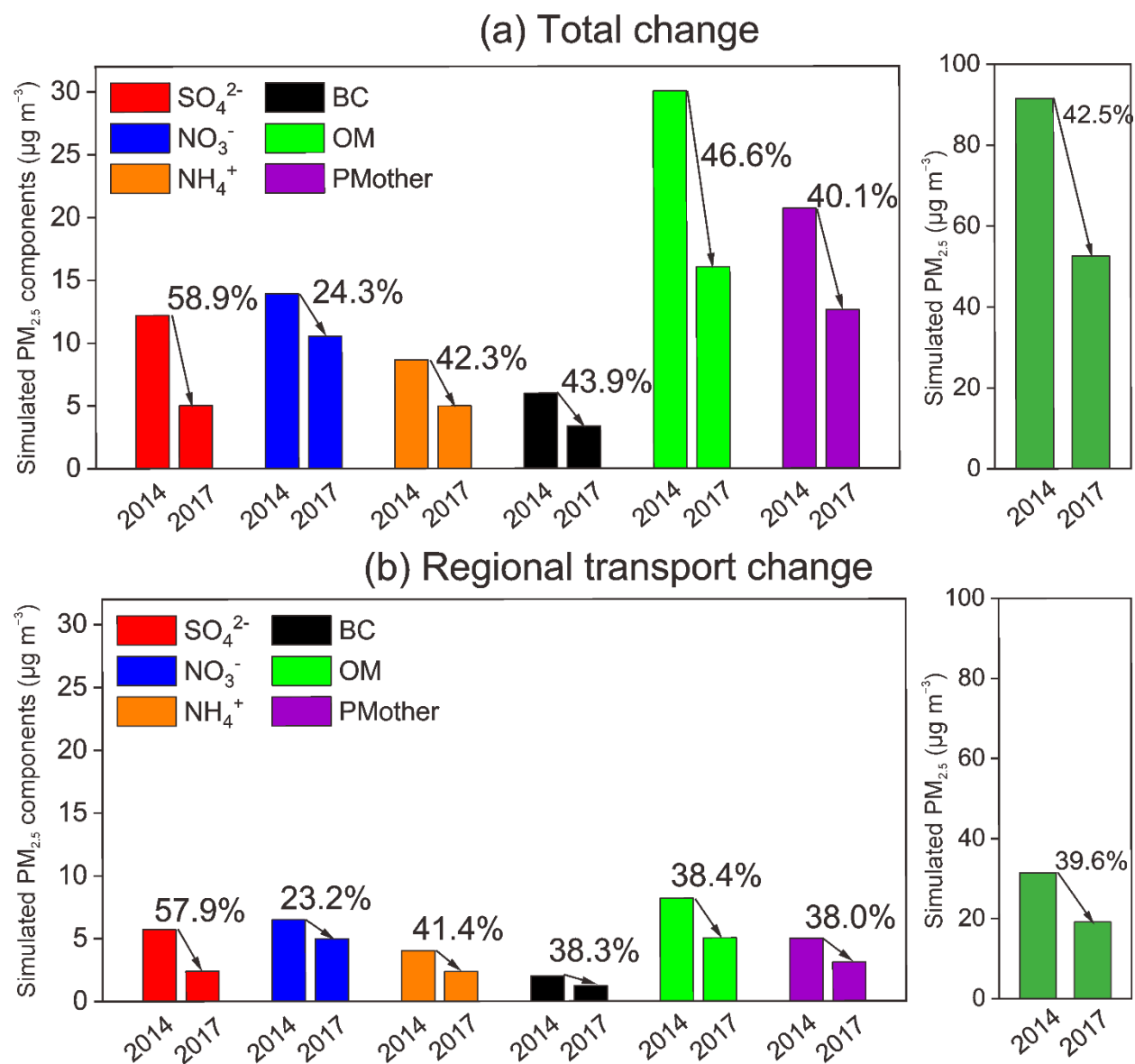
630 **Figure 3. Aerosol chemical composition at different pollution levels in the (a) winter of 2014 and (b) winter of 2017. The contributions of**  
 631 **each pollution level are shown at the top of each bar.**

(a) 2017 Emission+2017 Meteorology (b) 2017 Emission+2014 Meteorology



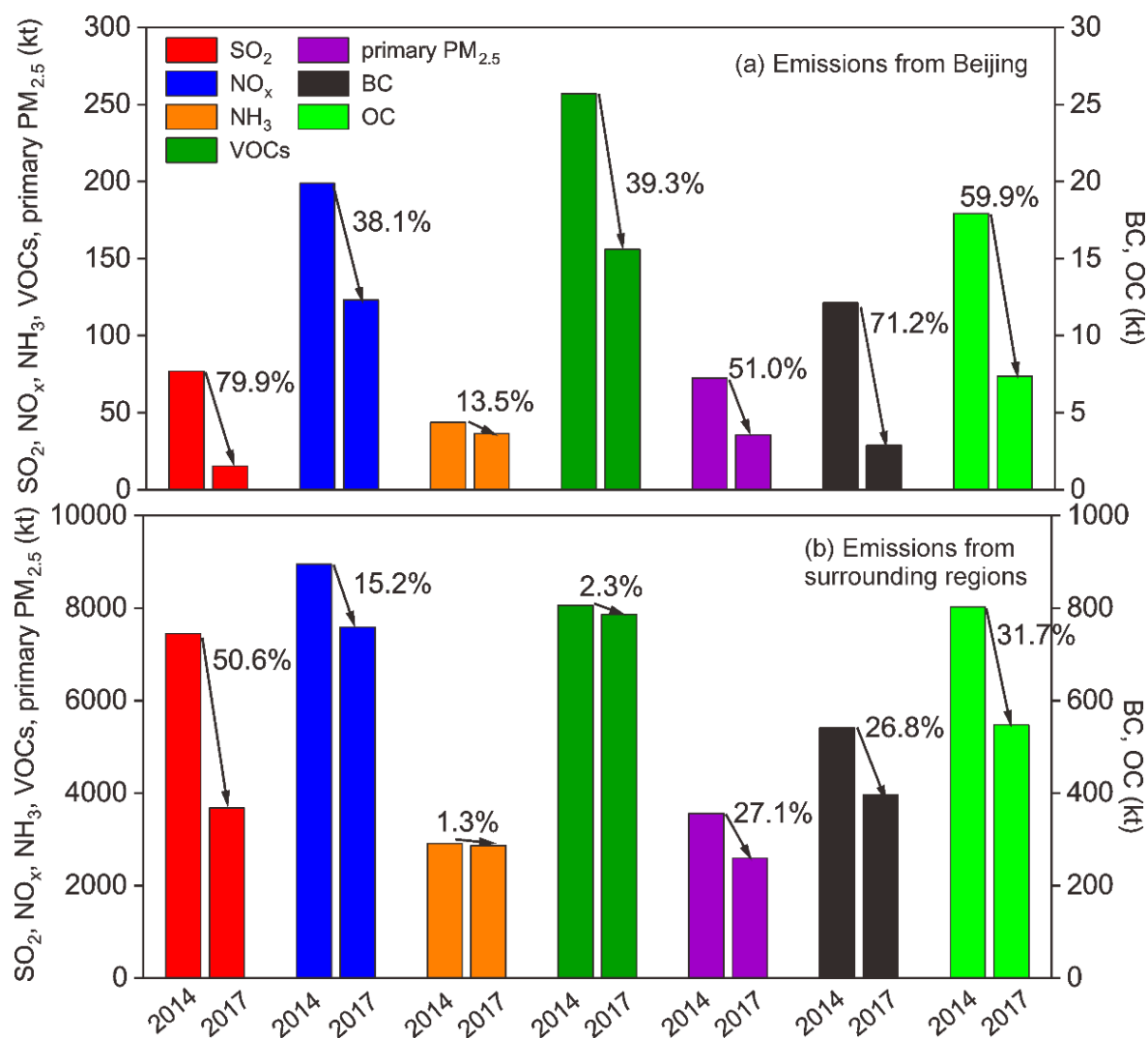
632

633 **Figure 4. The average PM<sub>2.5</sub> chemical composition simulated by the WRF-CMAQ model for the observation periods in 2017: (a) base**  
 634 **scenario with the 2017 emissions and the 2017 meteorological conditions; (b) simulation with the 2017 emissions and 2014 meteorological**  
 635 **conditions.**



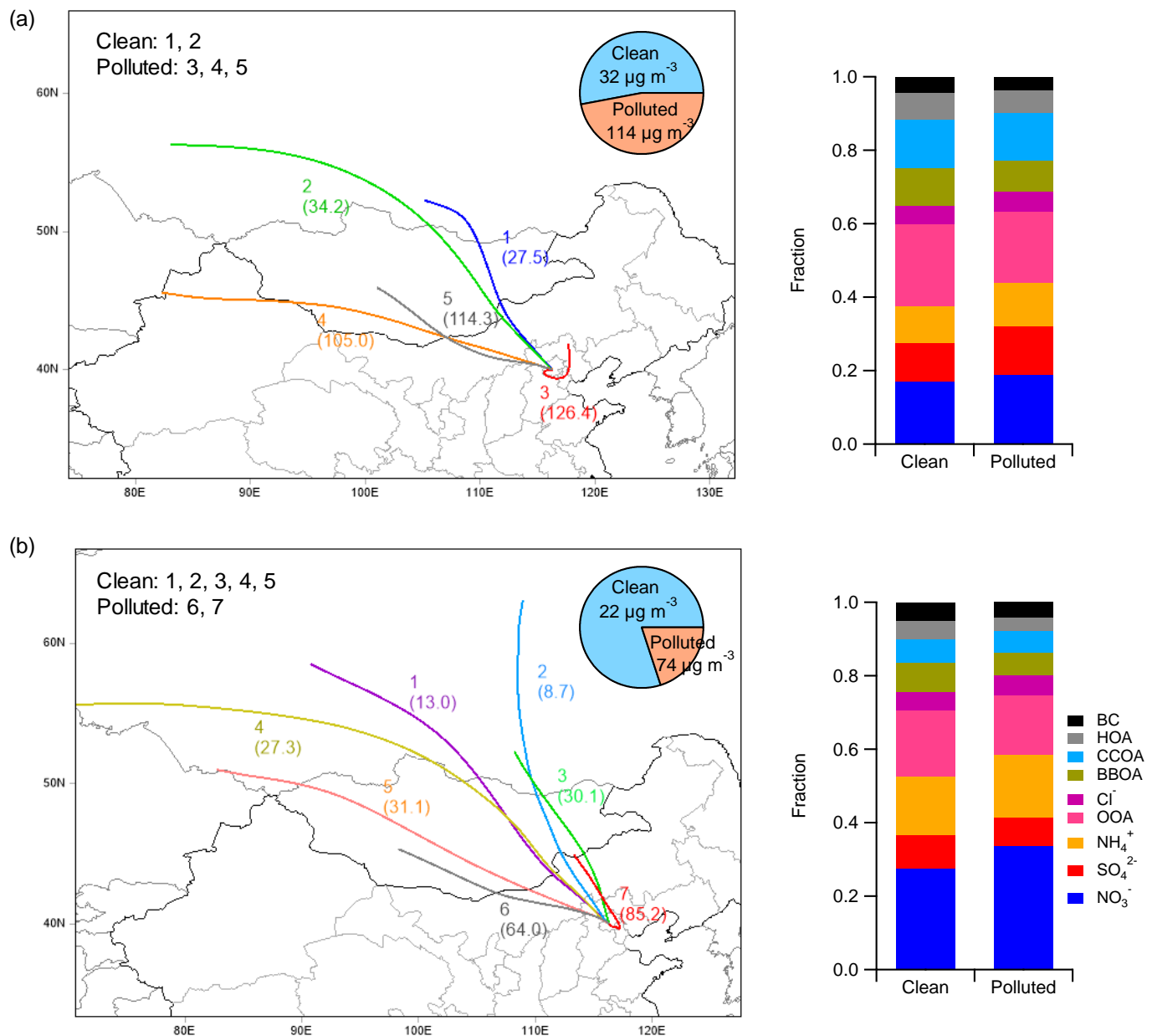
636

637 **Figure 5. Simulated concentrations of  $PM_{2.5}$  and its chemical components during the observation periods of 2014 and 2017: (a) total**  
 638 **changes in Beijing and (b) changes due to regional transport.**

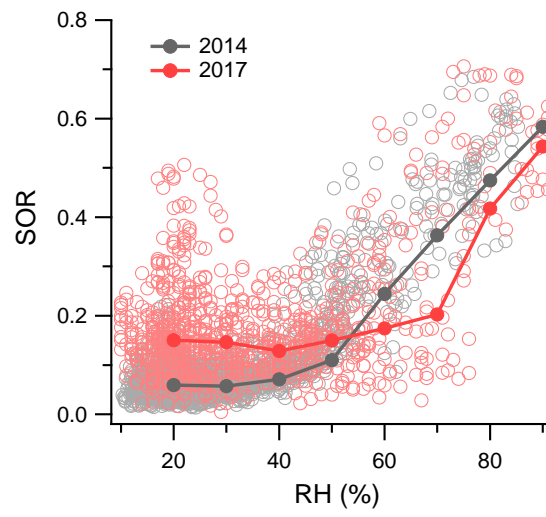


639

640 **Figure 6. Changes in the anthropogenic emissions of SO<sub>2</sub>, NO<sub>x</sub>, NH<sub>3</sub>, VOCs, primary PM<sub>2.5</sub>, BC, and OC in (a) Beijing and (b) its**  
 641 **surrounding regions from 2014 to 2017.**

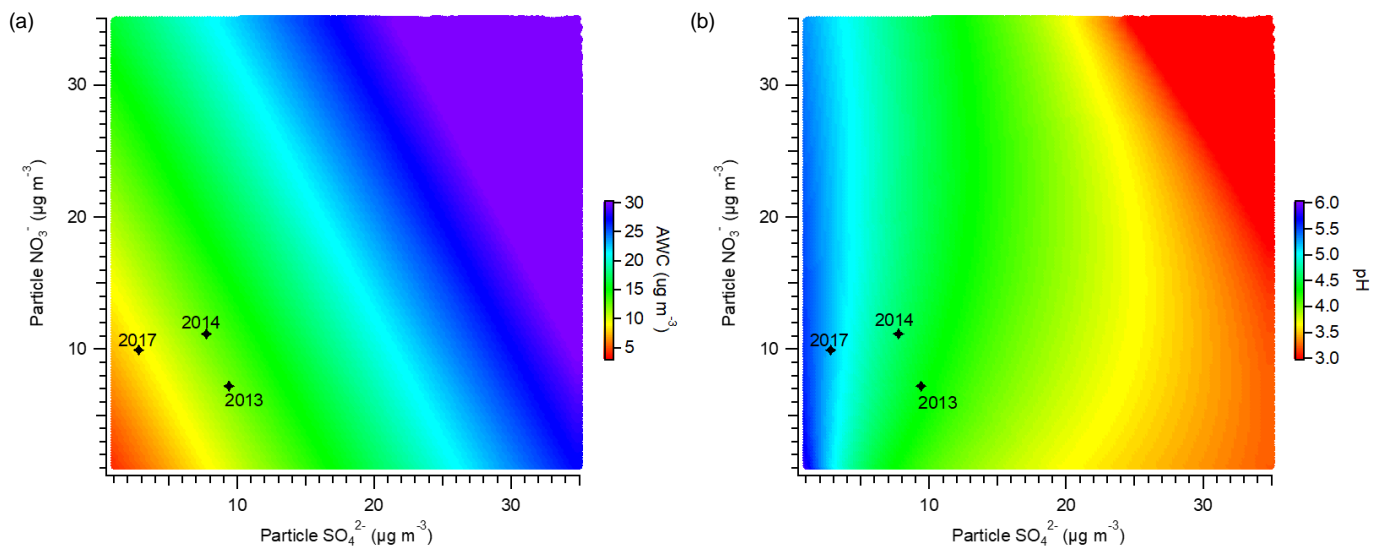






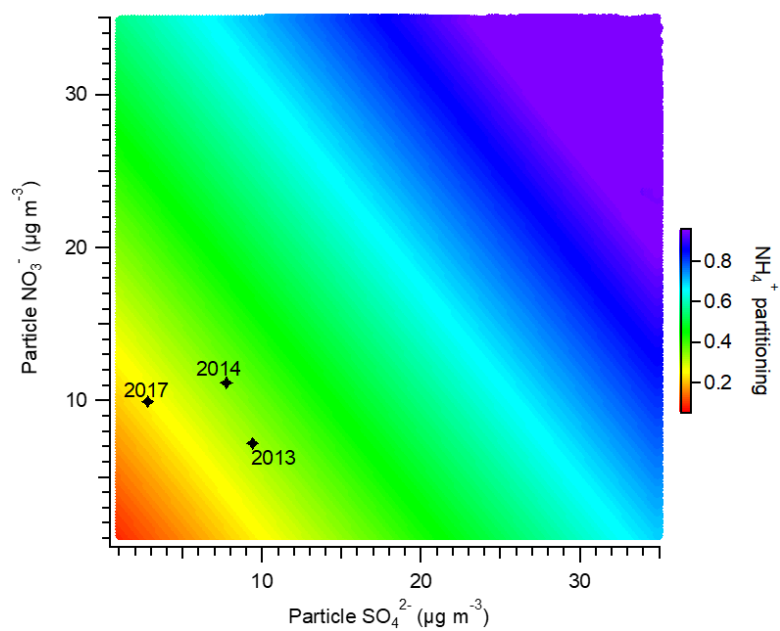
646

647 **Figure 8. Variations in SOR plotted against increasing RH. The data are also binned according to RH values, with the median value**  
 648 **shown for each bin.**



649

650 **Figure 9. Sensitivity of (a) AWC and (b) particle pH to the mass concentrations of particulate sulfate and nitrate. The stars indicate the**  
 651 **average winter conditions for the years 2013, 2014, and 2017.**



652

653 **Figure 10. Sensitivity of the ammonium partitioning ratio to the mass concentrations of particulate sulfate and nitrate. The stars indicate**  
 654 **the average winter conditions for the years 2013, 2014, and 2017.**